Photooxidative Generation of Dodecaborate-Based Weakly Coordinating Anions

Jonathan C. Axtell[1*], Marco S. Messina[1,2], Jiyuan Liu[3], Daria Galaktionova[4], Josef Schwan[5],

Tyler M. Porter[6], Miles Savage[1], Alex I. Wixtrom[1], Arnold L. Rheingold[6], Clifford P. Kubiak[6],

Jay R. Winkler[5], Harry B. Gray[5], Petr Král[4,7,8,*], Anastassia N. Alexandrova[1*], Alexander M.

Spokoyny[1,2,*]

[1]Department of Chemistry and Biochemistry, University of California, Los Angeles, 607 Charles E. Young Drive East, Los Angeles, California 90095-1569, United States.

[2] California NanoSystems Institute, University of California, Los Angeles, 570 Westwood Plaza, Los Angeles, California 90095-1569, United States.

[3] Key Laboratory for Advanced Materials, Center for Computational Chemistry and Research Institute of Industrial Catalysts, School of Molecular Science and Engineering, East China University of Science and Technology, Shanghai 200237 P.R. China

[4] Department of Chemistry, University of Illinois at Chicago, Chicago, IL 60607, United States

[5] Beckman Institute, California Institute of Technology, Pasadena, California, 91115, United States

[6] Department of Chemistry and Biochemistry, University of California, San Diego, 9500 Gilman Drive, La Jolla, California 92093, United States

[7] Department of Physics, University of Illinois at Chicago, Chicago, IL 60607, USA.

[8] Department of Biopharmaceutical Sciences, University of Illinois at Chicago, Chicago, IL 60607, USA.

Corresponding Authors: axtell@ucla.edu; spokoyny@chem.ucla.edu; pkral@uic.edu; ana@chem.ucla.edu, hbgray@caltech.edu.

Table of Contents

General Considerations. All commercially available chemicals were used as received unless otherwise stated. All polymerizations were prepared in the glovebox under nitrogen atmosphere unless otherwise stated. CH3CN used for oxidations of **1 – 3** was purified via a solvent purification system and kept in the glovebox. All monomers were degassed and stored with 4Å molecular sieves. 4-Vinylanisole (97%), 4-methylstyrene (96%), styrene (≥99%), 4-fluorostyrene (99%), 4-*tert*-butylstyrene (93%), 4-chlorostyrene (97%), 3-chlorostyrene (98%), and 2,6-difluorostyrene (99%) were purchased from Sigma-Aldrich. Acetonitrile (≥99.9%), dichloromethane (≥99.5%), ethyl acetate (≥99.5%), hexanes (≥98.5%), methanol (≥99.8%), N,N-diisopropylethylamine (≥99%), and tetrabutylammonium hexafluorophosphate (≥99.0%, electrochemical grade) were purchased from Sigma-Aldrich. Tetrabutylammonium hexafluorophosphate was further purified by recrystallization from ethanol and drying under vacuum at 90 °C and benzyl bromide (99%) was purchased from Alfa Aesar. Perfluorotoluene (TCI) was dried 72h over 3Å molecular sieves and degassed prior to use. $[NBu_4]_2B_{12}(OH)_{12}$ was synthesized according to reported procedures.[1]

NMR spectra were recorded using spectrometers at 400 or 500 MHz (^{1}H), 125 MHz (^{13}C), 80 MHz (^{11}B), and 282 MHz (^{19}F) reported in δ (parts per million) relative to tetramethylsilane (^{1}H, ^{13}C), $BF_3 \cdot Et_2O$ (^{11}B), and C_6H_5F (^{19}F), respectively, and referenced to residual ^{1}H/^{13}C signals of the deuterated solvent (^{1}H (δ) CDCl$_3$ 7.26; ^{13}C (δ) CDCl$_3$ 77.16; ^{11}B (δ) $BF_3 \cdot Et_2O$ 0.00 ppm; ^{19}F (δ) C_6H_5F -113.15 ppm). Deuterated solvents (Cambridge Isotope Laboratories) for NMR spectroscopic analyses were stored over 4Å molecular sieves. ^{1}H NMR spectra were acquired with a relaxation of 2 s for small molecules and 30 s for polymers. Gel permeation chromatography (GPC) for all polymers was conducted on a Shimadzu HPLC Prominence-i system equipped with a UV detector, Wyatt DAWN Heleos-II Light Scattering detector, Wyatt Optilab T-rEX RI detector, one MZ-Gel SDplus guard column, and two MZ-Gel SDplus 100 Å 5μm 300x8.0 mm columns. Eluent was CHCl$_3$ or THF at 40 °C (flow rate: 0.70 mL/min), a dn/dc value of 0.160 was used for chloroform and 0.1828 was used for samples in THF. GPC chromatograms were analyzed using Astra 6.0 software. All GPC samples were dissolved in HPLC grade solvent at a concentration of 4-5 mg/mL and filtered through a 0.2 μm TFE filter. All reported molecular weight and dispersity data determined by GPC are the average of two runs unless otherwise noted. Mass spectrometry data was acquired using a Thermo Scientific™ Q-Exactive™ Plus instrument with a quadrupole mass filter and Orbitrap mass analyzer. UV-Vis spectra were recorded on a Hewlett-Packard 8453 diode array spectrometer. Extinction coefficients were determined through a series of 5 dilutions with a maximum absorption between 0.1 and 0.7 absorbance units. Microwave reactions were performed using a CEM Discover SP microwave synthesis reactor at 140 °C with the pressure release limit set to 250 psi (no reactions exceeded this limit to trigger venting) and the maximum wattage set to 250W (the power applied was dynamically controlled by the microwave instrument and did not exceed this limit for any reactions). Irradiation of photochemical polymerizations were performed utilizing a 120V Blue LED Custom Rope Light Kit 1⁄2" 2 wire 3 foot cable purchased from Novelty Lights, Inc. (Eaglewood, CO).

Note: **1**[2] and **2**[3] were previously synthesized using FeCl$_3$. An improved synthesis employing NOBF$_4$ as the oxidant is reported here and the resulting products are spectroscopically identical to those of the initial reports. The synthesis of **3** was recently published[4] and is reported here for simplicity.

$B_{12}(OCH_2C_6F_5)_{12}$ (1). $TBA_2[B_{12}(OH)_{12}]$ (2.00 g, 2.44 mmol) was transferred out of a nitrogen filled glovebox, opened to the air, and dissolved in 20 mL acetonitrile in an 80 mL glass microwave vial. *N,N*-diisopropylethylamine (8 mL, 45.93 mmol) and 2,3,4,5,6-pentafluorobenzyl bromide (12.0 mL, 79.45 mmol) were added along with a stir bar, the vial was sealed with the large vial attachment kit lid, and the mixture was heated at 140 °C with stirring in the microwave for 45 min. The volatiles were removed *via* rotary evaporation, and the resulting residue was loaded on a slurry-packed silica gel column with 65/35 hexanes/ethyl acetate eluent ratio. The excess reagents eluted first, and the pink/purple product mixture was eluted with acetone. The acetone was removed *via* rotary evaporation and the resulting residue (a mixture of $[B_{12}(OCH_2C_6F_5)_{12}]^{2-}$ and $[B_{12}(OCH_2C_6F_5)_{12}]^{1-}$) was dissolved in minimal acetonitrile (~30 mL). $NOBF_4$ (0.67 g, 5.7 mmol) was added and the mixture was left to stir for 48 h. Following oxidation, the product was filtered and washed with cold CH_3CN (3 x 15 mL) and the yellow-orange solid was dried under high vacuum (5.22 g, 86%). ^1H NMR (500 MHz, $CDCl_3$): δ 5.23 (s, 24H). ^{13}C NMR (125 MHz, $CDCl_3$): δ 60.1. ^{11}B NMR (160 MHz, $CDCl_3$): δ 40.9.

$B_{12}(OCH_2C_7H_4F_3)_{12}$ (2). $TBA_2[B_{12}(OH)_{12}]$ (1.00 g, 1.22 mmol) was transferred out of a nitrogen filled glovebox, opened to the air, and dissolved in 10 mL acetonitrile in an 80 mL glass microwave vial. *N,N*-diisopropylethylamine (4.00 mL, 23.0 mmol) and 4-trifluoromethylbenzyl bromide (7.22mL, 46.7 mmol) were added along with a stir bar, the vial was sealed with the large vial attachment kit lid, and the mixture was heated at 140 °C with stirring in the microwave for 45 min. The volatiles were removed *via* rotary evaporation, and the resulting residue was loaded on a slurry-packed silica gel column with a 65/35 hexanes/ethyl acetate eluent ratio. The excess reagents eluted first, and the pink/purple product mixture was eluted with acetone. The acetone was removed *via* rotary evaporation and the resulting residue (a mixture of $[B_{12}(OCH_2\text{-}4\text{-}CF_3\text{-}C_6H_4)_{12}]^{2-}$ and $[B_{12}(OCH_2\text{-}4\text{-}CF_3\text{-}C_6H_4)_{12}]^{1-}$) was dissolved in a minimal volume of acetonitrile (~15 mL). $NOBF_4$ (0.658 g, 5.63 mmol) was added and the mixture was left to stir for 24 h. The resulting mixture was then cooled at -30°C for 30min, and the red-orange solid was isolated *via* filtration, washed with cold CH_3CN, and dried under high vacuum (1.82 g, 69%). ^1H NMR (400 MHz, $CDCl_3$): δ 7.41 (d, 24H, Ar), 7.09 (d, 24H, Ar), 5.27 (s, 24H, CH_2); ^{11}B NMR (160 MHz) 41.70; ^{19}F NMR (282 MHz) -62.73.

$B_{12}(OCH_2\text{-}3,5\text{-}(CF_3)_2\text{-}C_6H_3)_{12}$ (3). $TBA_2[B_{12}(OH)_{12}]$ (1.00 g, 1.22 mmol) was transferred out of a nitrogen filled glovebox, opened to the air, and dissolved in 10 mL acetonitrile in an 80 mL glass microwave vial. *N,N*-diisopropylethylamine (4 mL, 23.0 mmol) and 3,5-bis(trifluoromethyl)benzyl bromide (8.0 mL, 44.0 mmol) were added along with a stir bar, the vial was sealed with the large vial attachment kit lid, and the mixture was heated at 140 °C with stirring in the microwave for 45 min. The volatiles were removed *via* rotary evaporation, and the resulting residue was loaded on a slurry-packed silica gel column with 65/35 hexanes/ethyl acetate eluent ratio. The excess reagents eluted first, and the pink/purple product mixture was eluted with acetone. The acetone was removed *via* rotary evaporation and the resulting residue (a mixture of $[B_{12}(OCH_2\text{-}3,5\text{-}(CF_3)_2\text{-}C_6H_3)_{12}]^{2-}$ and $[B_{12}(OCH_2\text{-}3,5\text{-}(CF_3)_2\text{-}C_6H_3)_{12}]^{1-}$) was dissolved in a minimal volume of acetonitrile (~15 mL). $NOBF_4$ (0.436 g, 3.73 mmol) was added and the mixture was left to stir for 24 h. Following oxidation, the red-orange solid was isolated via filtration, washed with cold CH_3CN (3 x 15 mL), and dried under high vacuum (2.93 g, 79%). ^1H NMR (400 MHz, CD_2Cl_2): δ 7.80 (br s, 12H, Ar), 7.55 (br s, 24H, C_6H_3), 5.49 (s, 24H, CH_2). $^{11}B\{^1H\}$ NMR (128 MHz, CD_2Cl_2): δ 42.4. ^{19}F NMR (282 MHz, CD_2Cl_2): δ -63.97 (s, 72F).

Representative Styrene Polymerization:
Styrene (0.05 mL, 0.435 mmol) was passed through activated basic alumina and added to a dram vial equipped with a magnetic stir bar. **1** (1.1 mg, 0.1 mol%) was then added. This mixture was dissolved in 219 µL dichloromethane, affording a 2M solution of monomer. The dram vial was sealed with a polypropylene cap containing a Teflon coated septum and brought out of the glove box. The mixture was then irradiated with blue LED light (450 nm) while stirring for 4 hours at room temperature. For all reactions, the reaction setup is covered with aluminum foil to keep out ambient light. Once the polymerization was complete, the reaction was diluted with ~500 µL dichloromethane and precipitated with cold methanol. The resulting suspension was transferred to a tared falcon tube and centrifuged for 5 minutes at 4,400 RPM. The supernatant was discarded, methanol was then added, stirred to solubilize any excess oxidant, and centrifuged again. The supernatant was discarded and the polymer was dried under vacuum.

Polymer Characterization Data
Note: Polymerizations of S1, S2, S3, and S5 in CH_2Cl_2 were previously reported.[2]
Table S1. Summary of polymer data.

	CH_2Cl_2								
	2			**1**			**3**		
	$M_n(M_w)$ (kDa)	PDI	Yield (%)	$M_n(M_w)$ (kDa)	PDI	Yield (%)	$M_n(M_w)$ (kDa)	PDI	Yield (%)
S1	6.90(13.3)	1.9	57	8.4	2.3	96	7.40(16.4)	2.2	86
	6.90(14.6)	2.1	65				7.70(17.1)	2.3	86
S2	14.8(30.3)	2	89	170	2.4	99	12.3(21.5)	1.7	92
	15.5(30.3)	1.9	77				5.40(15.2)	2.8	62
S3	53.2(130.6)	2.5	89	227	3.2	94	88.3(279.1)	3.2	94
	103.4(266.6)	2.6	84				96.3(296.9)	3.1	89
S4	54.7(100.8)	1.8	88	138.18(305.8)	2.2	95	44(83.9)	1.9	91
	58.3(102.9)	1.8	85	141.64(300.7)	2.12	99	46(76.5)	1.7	98
S5	137.5(358.1)	2.6	96	76.9	2.6	98	67.9(146.5)	1.9	99
	134.2(356.4)	2.7	90				82.1(171.8)	2.1	87
S6	NA	NA	<1	6.48(9.6)	1.49	33	NA	NA	<1
	NA	NA	<1	6.71(9.9)	1.48	24	NA	NA	<1

	$1,2-F_2Ph$								
	2			**1**			**3**		
	$M_n(M_w)$ (kDa)	PDI	Yield (%)	$M_n(M_w)$ (kDa)	PDI	Yield (%)	$M_n(M_w)$ (kDa)	PDI	Yield (%)
S1	8.50(16.1)	1.9	81	19.3(40)	2.07	94	5.80(10.6)	1.8	85
	6.90(14.6)	2.1	87	20.2(42.7)	2.11	94	5.60(10.9)	1.9	77
S2	6.30(9.70)	1.5	61	25.6(59.9)	2.34	74	8.00(13.1)	1.6	85
	6.30(9.80)	1.6	69	32.7(70.5)	2.15	88	7.9(13.4)	1.7	83
S3	74.2(139.6)	1.9	40	73.7(129.0)	1.75	95	113.1(267.1)	2.4	97
	54.8(124.3)	2.3	75	56.2(116.4)	2.07	Quant	47.5(121.4)	2.6	89
S4	62.8(113.3)	1.81	89	36.8(67.8)	1.84	88	50.46(97.8)	1.94	98
	60.7(109)	1.8	84	23.1(57.9)	2.51	99	39.49(83.7)	2.11	99
S5	56(79.4)	1.42	93	62.3(125.1)	2.01	Quant	52.4(82)	1.56	94
	55.9(78.4)	1.4	89	75.5(130.5)	1.73	Quant	50.9(81.5)	1.6	95
S6	5.9(9.7)	1.63	25	6.1(10.4)	1.7	84%	7.68(8.6)	1.12	65
	4.4(8.1)	1.86	36	6.9(10.7)	1.56	85%	7.52(8.6)	1.14	80

Polymerizations initiated by **1**:

Sample	M_n (kDa)	M_w (kDa)	Đ
—— (black)	20.2	42.7	2.1
—— (red)	19.3	40.0	2.1
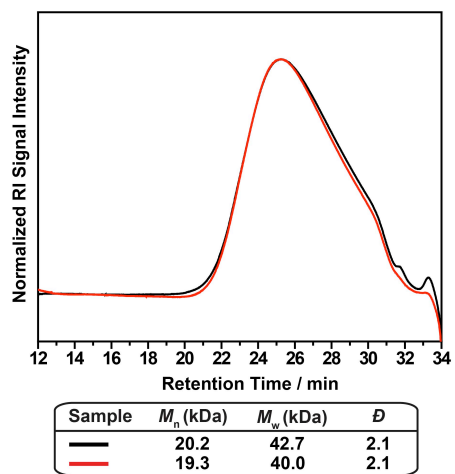
Figure S1. Styrene, 1,2-difluorobenzene.

Sample	M_n (kDa)	M_w (kDa)	Đ
—— (black)	25.6	59.9	2.3
—— (red)	32.7	70.5	2.2
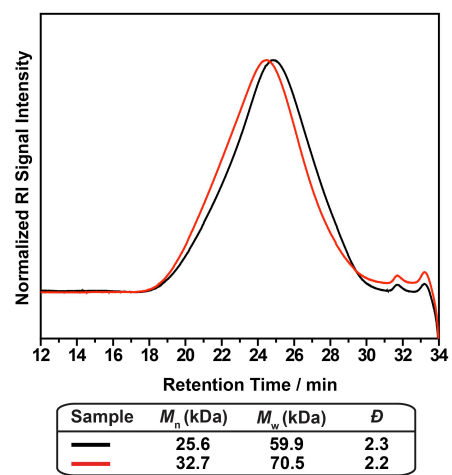
Figure S2. 4-fluorostyrene, 1,2-difluorobenzene.

Sample	M_n (kDa)	M_w (kDa)	Đ
	56.2	116.4	2.1
	73.7	129.0	1.8
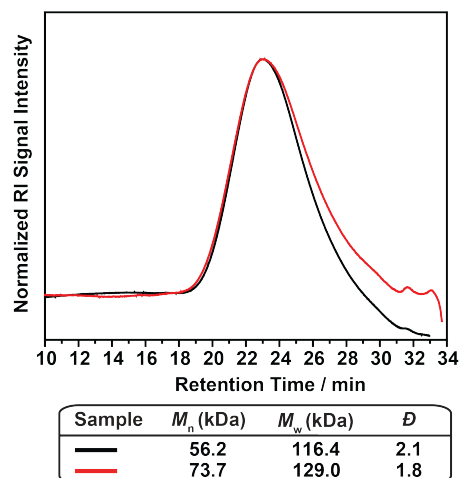
Figure S3. 4-chlorostyrene, 1,2-difluorobenzene.

Sample	M_n (kDa)	M_w (kDa)	Đ
	138.2	305.8	2.2
	141.6	300.7	2.1
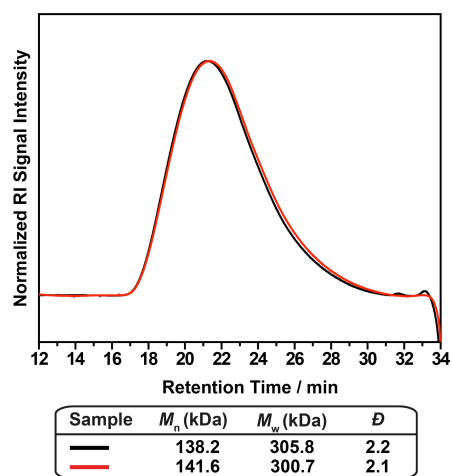
Figure S4. 4-bromostyrene, CH_2Cl_2

Sample	M_n (kDa)	M_w (kDa)	Đ
——— (black)	36.8	67.8	1.8
——— (red)	23.1	57.9	2.5
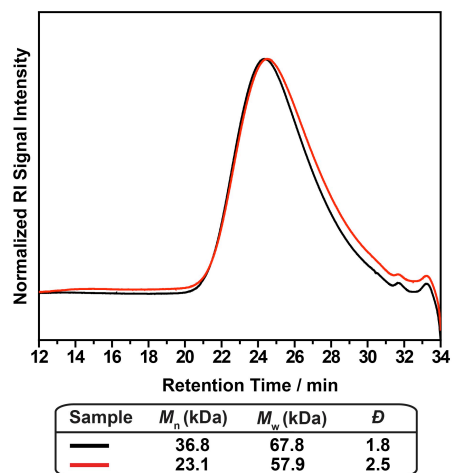
Figure S5. 4-bromostyrene, 1,2-difluorobenzene.

Sample	M_n (kDa)	M_w (kDa)	Đ
——— (black)	62.9	121.1	2.0
——— (red)	75.5	130.5	1.7
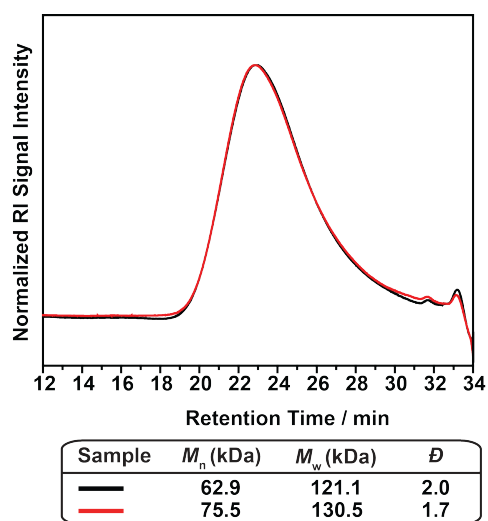
Figure S6. 2,4,6-trimethylstyrene, 1,2-difluorobenzene.

Sample	M_n (kDa)	M_w (kDa)	Đ
—	6.71	9.94	1.5
—	6.48	9.62	1.5

Figure S7. 2-vinylnapthalene, CH_2Cl_2.

Sample	M_n (kDa)	M_w (kDa)	Đ
—	6.15	10.4	1.7
—	6.85	10.7	1.6
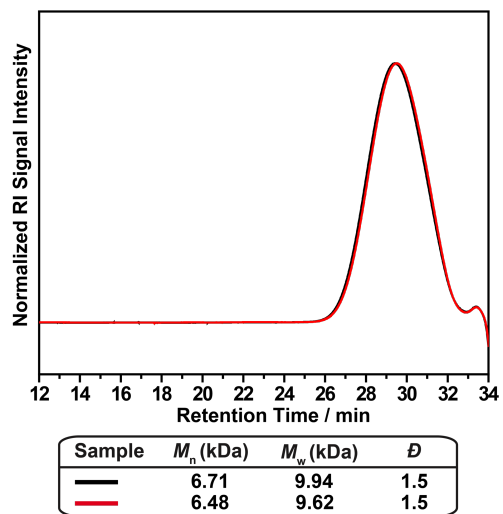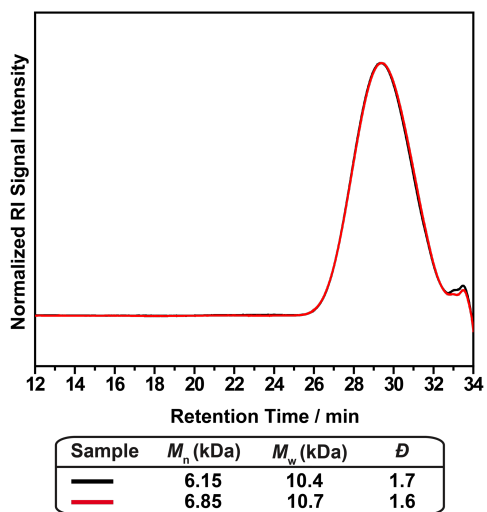
Figure S8. 2-vinylnapthalene, 1,2-difluorobenzene.

Polymerizations initiated by **2**:

Sample	M_n (kDa)	M_w (kDa)	Đ
——	6.90	13.3	1.9
——	6.90	14.6	2.1
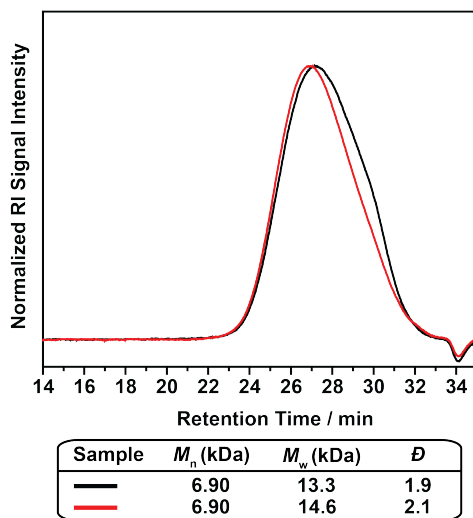
Figure S9. Styrene, CH_2Cl_2.

Sample	M_n (kDa)	M_w (kDa)	Đ
——	8.50	16.1	1.9
——	7.40	15.1	2.1
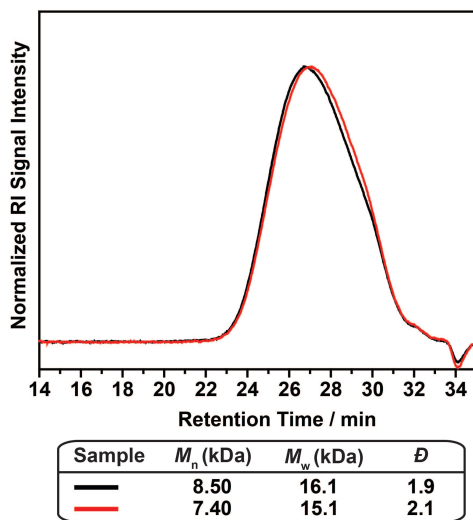
Figure S10. Styrene, 1,2-difluorobenzene.

Sample	M_n (kDa)	M_w (kDa)	Đ
———	14.8	30.3	2.0
———	15.5	30.3	1.9
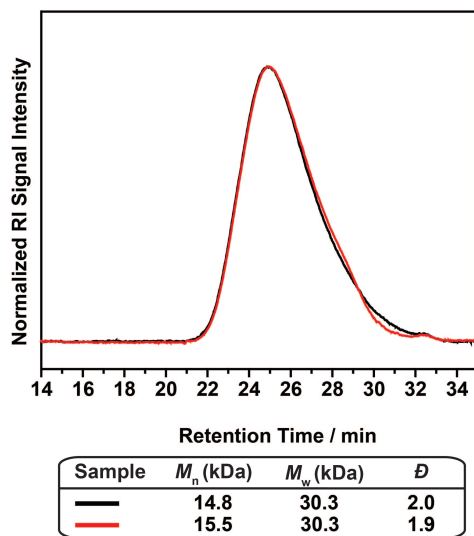
Figure S11. 4-fluorostyrene, CH$_2$Cl$_2$.

Sample	M_n (kDa)	M_w (kDa)	Đ
———	6.30	9.70	1.5
———	6.30	9.80	1.6
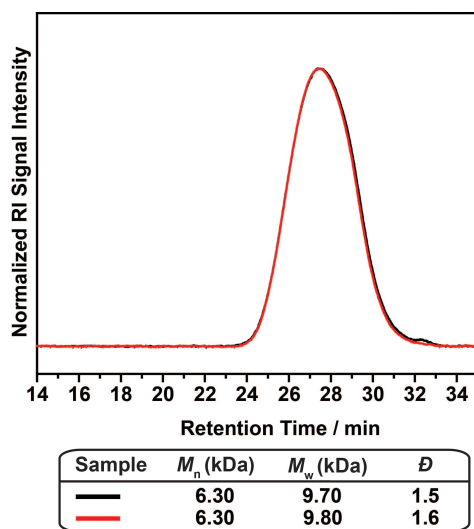
Figure S12. 4-fluorostyrene, 1,2-difluorobenzene.

Sample	M_n (kDa)	M_w (kDa)	Đ
(black)	53.2	130.6	2.5
(red)	103.4	266.6	2.6
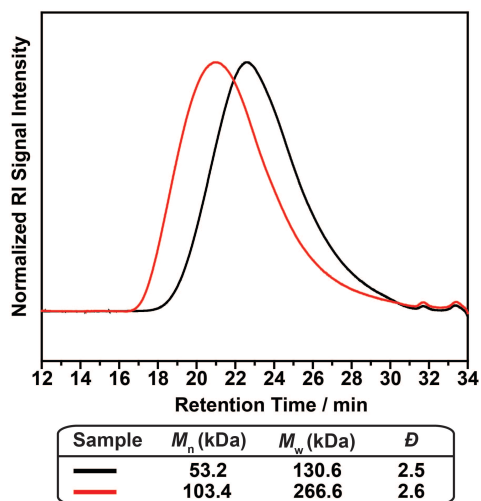
Figure S13. 4-chlorostyrene, CH_2Cl_2.

Sample	M_n (kDa)	M_w (kDa)	Đ
(black)	74.2	139.6	1.9
(red)	54.8	124.3	2.3
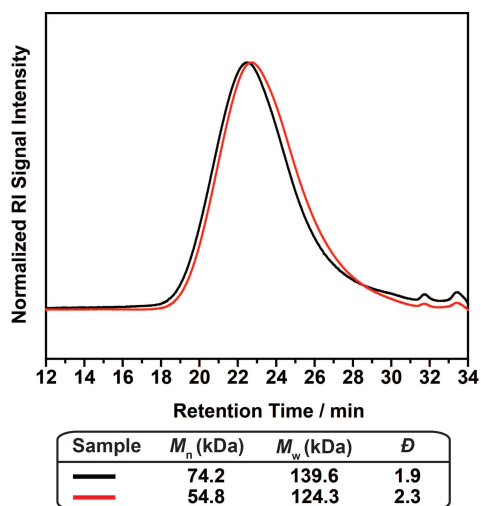
Figure S14. 4-chlorostyrene, 1,2-difluorobenzene.

Sample	M_n (kDa)	M_w (kDa)	Đ
	62.8	113.3	1.8
	60.7	109.0	1.8
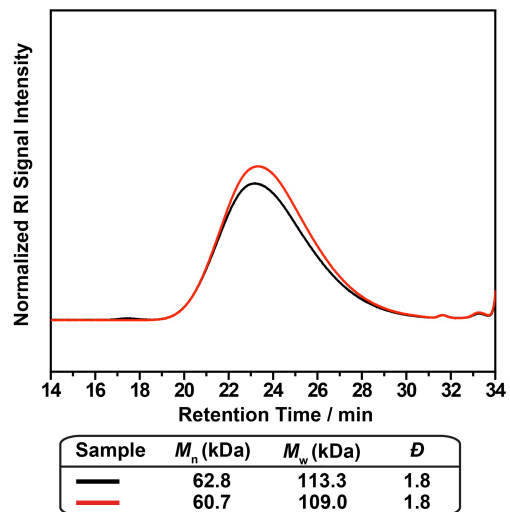
Figure S15. 4-bromostyrene, 1,2-difluorobenzene.

Sample	M_n (kDa)	M_w (kDa)	Đ
	56.0	79.4	1.4
	55.9	78.4	1.4
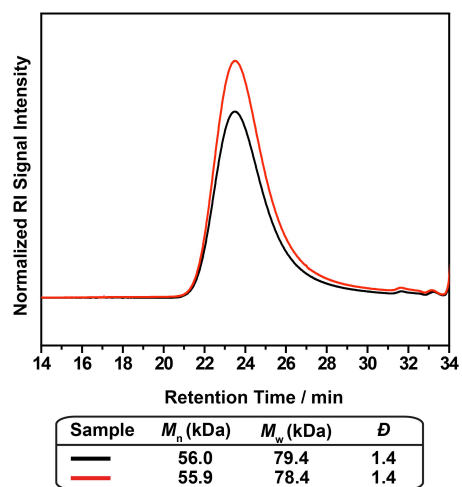
Figure S16. 2,4,6-trimethylstyrene, 1,2-difluorobenzene.

Sample	M_n (kDa)	M_w (kDa)	Đ
▬	5.90	9.70	1.6
▬	4.40	8.10	1.9
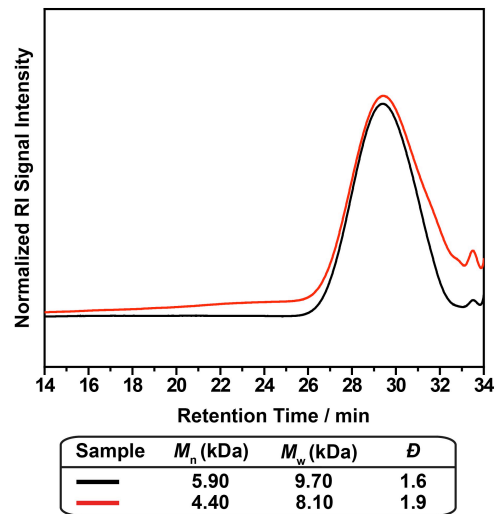
Figure S17. 2-vinylnaphthalene, 1,2-difluorobenzene.

Sample	M_n (kDa)	M_w (kDa)	Đ
▬	58.3	102.9	1.8
▬	54.7	100.8	1.8
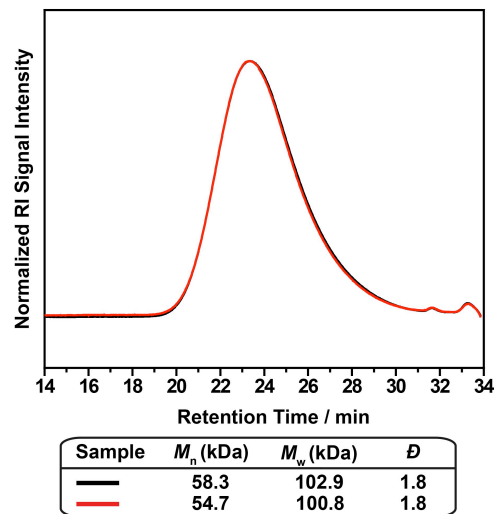
Figure S18. 4-bromostyrene, CH_2Cl_2.

Sample	M_n (kDa)	M_w (kDa)	Đ
———	137.5	358.1	2.6
———	134.2	356.4	2.7
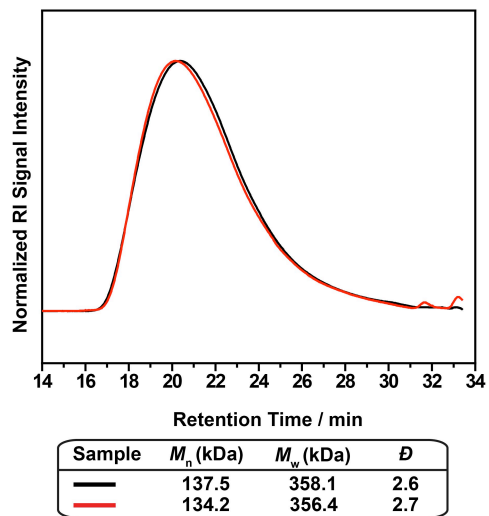
Figure S19. 2,4,6-trimethylstyrene, CH_2Cl_2.

Polymerizations initiated by **3**:

Sample	M_n (kDa)	M_w (kDa)	Đ
(black)	7.40	16.4	2.2
(red)	7.70	17.1	2.3
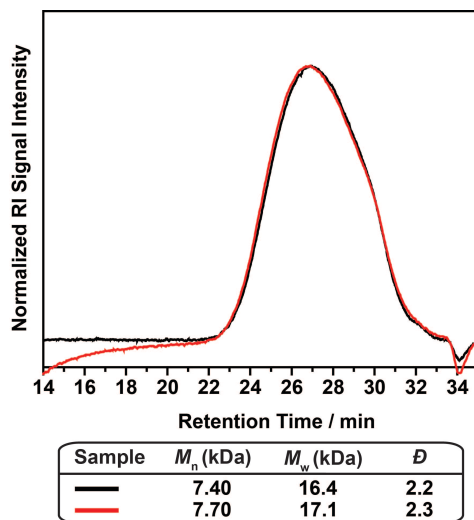
Figure S20. Styrene, CH_2Cl_2.

Sample	M_n (kDa)	M_w (kDa)	Đ
(black)	5.80	10.6	1.8
(red)	5.60	10.9	1.9
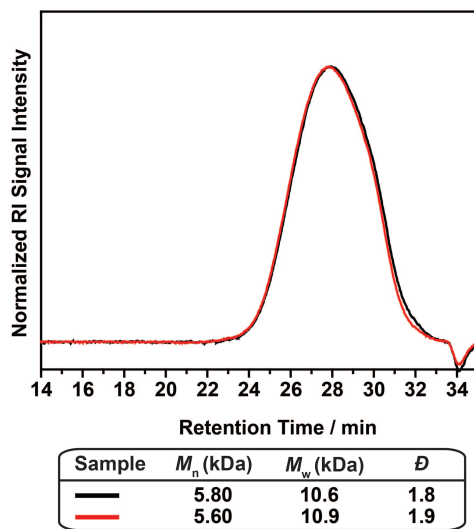
Figure S21. Styrene, 1.2-difluorobenzene.

Sample	M_n (kDa)	M_w (kDa)	Đ
▬	12.3	21.5	1.7
▬	5.40	15.2	2.8
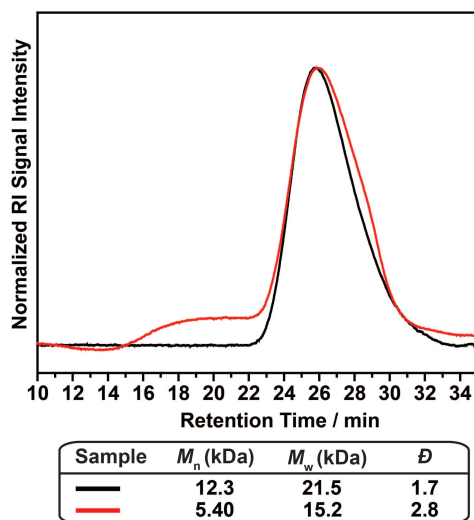
Figure S22. 4-fluorostyrene, CH_2Cl_2.

Sample	M_n (kDa)	M_w (kDa)	Đ
▬	8.00	13.1	1.6
▬	7.90	13.4	1.7
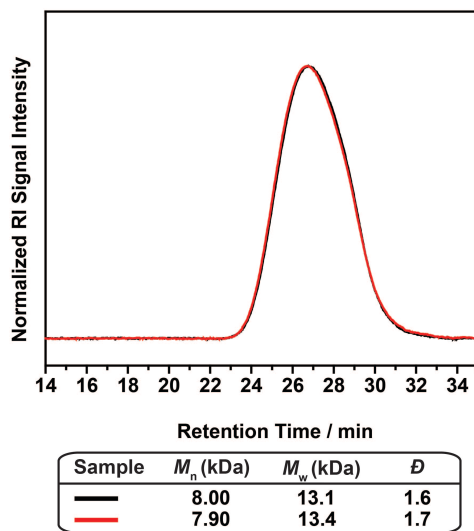
Figure S23. 4-fluorostyrene, 1,2-difluorobenzene.

Sample	M_n (kDa)	M_w (kDa)	Đ
(black)	88.3	279.1	3.2
(red)	96.3	296.9	3.1
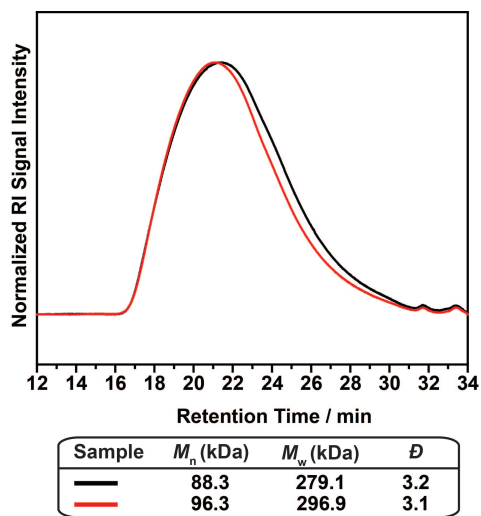
Figure S24. 4-chlorostyrene, CH_2Cl_2.

Sample	M_n (kDa)	M_w (kDa)	Đ
(black)	113.1	267.1	2.4
(red)	47.5	121.4	2.6
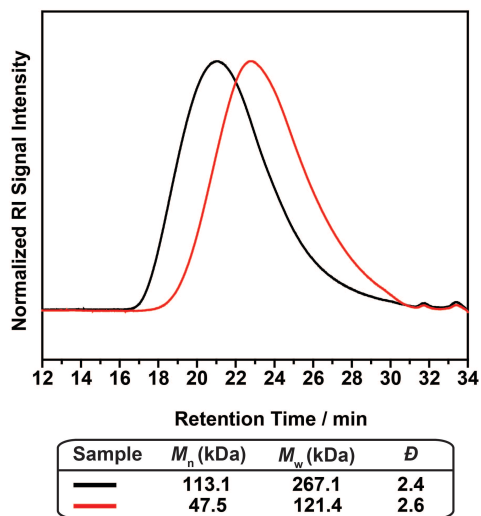
Figure S25. 4-chlorostyrene, 1,2-difluorobenzene.

Sample	M_n (kDa)	M_w (kDa)	Đ
⎯⎯	46.1	76.5	1.7
⎯⎯	44.0	83.9	1.9
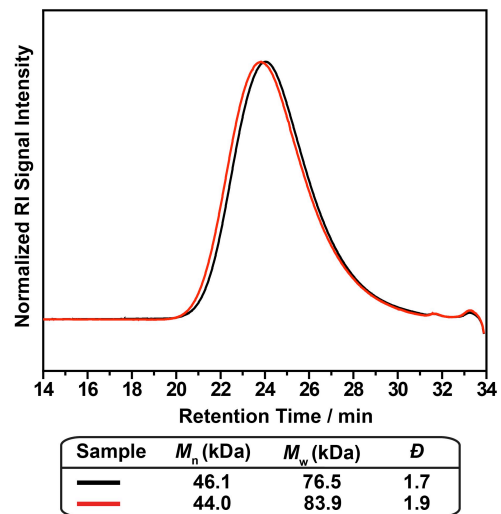
Figure S26. 4-bromostyrene, CH_2Cl_2.

Sample	M_n (kDa)	M_w (kDa)	Đ
⎯⎯	50.5	97.8	1.9
⎯⎯	39.5	83.7	1.9
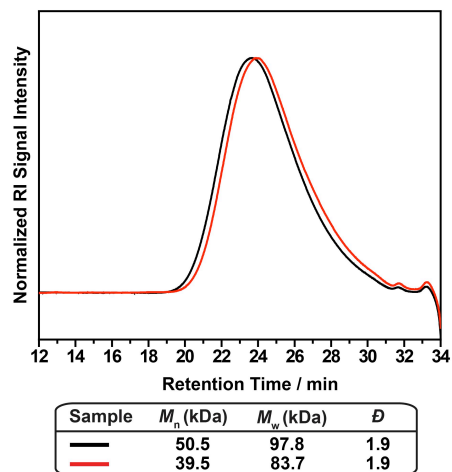
Figure S27. 4-bromostyrene, 1,2-difluorobenzene.

Sample	M_n (kDa)	M_w (kDa)	Đ
⚫	67.9	146.5	2.2
🔴	82.1	171.8	2.1
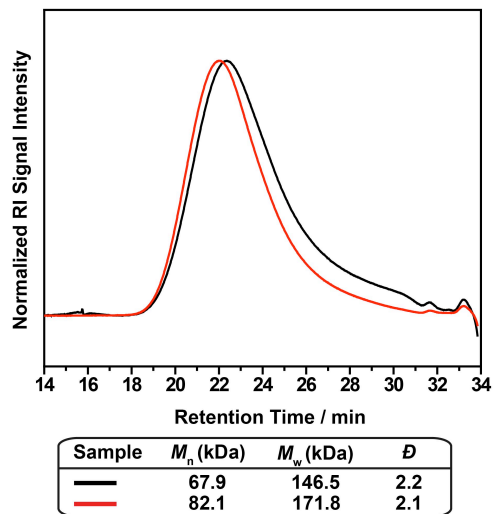
Figure S28. 2,4,6-trimethylstyrene, CH_2Cl_2.

Sample	M_n (kDa)	M_w (kDa)	Đ
⚫	52.4	82.0	1.6
🔴	50.9	81.5	1.6
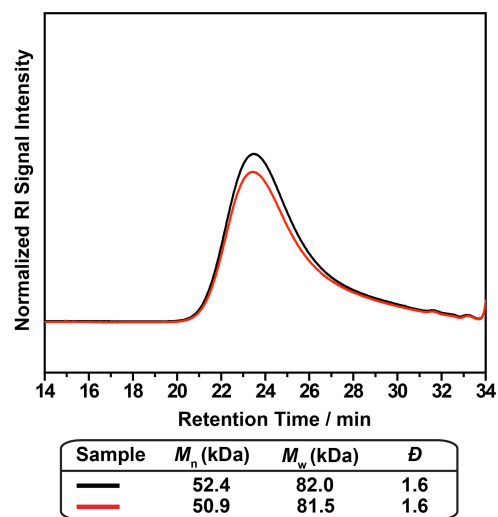
Figure S29. 2,4,6-trimethylstyrene, 1,2-difluorobenzene.

Sample	M_n (kDa)	M_w (kDa)	Đ
——	7.68	8.60	1.1
——	7.52	8.61	1.1
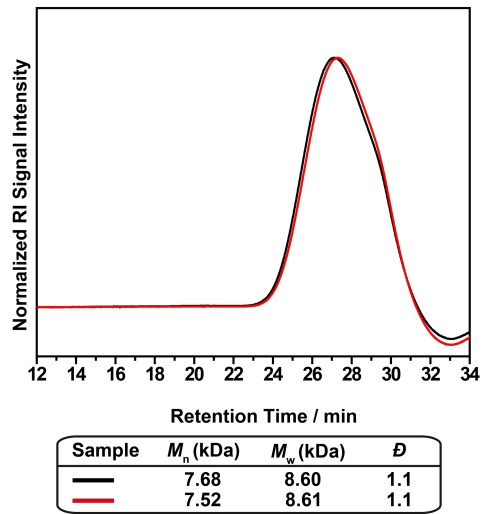
Figure S30. 2-vinylnaphthalene, 1,2-difluorobenzene.

Sample	M_n (kDa)	M_w (kDa)	Đ
——	16.9	38.8	2.3
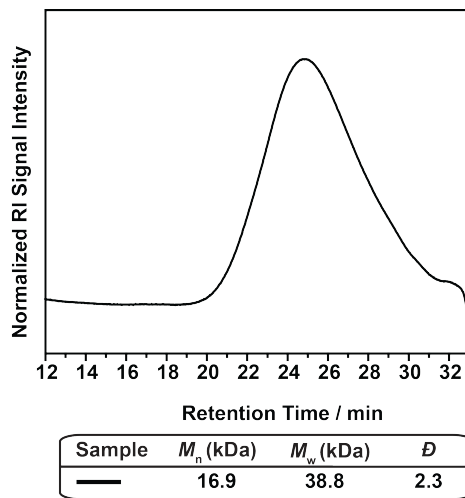
Figure S31. Styrene, **3**, 1,2-difluorobenzene, 1 equiv. [NBu4]BArF4.

Sample	M_n (kDa)	M_w (kDa)	Đ
▬ (black)	15.1	30.6	2.4
▬ (red)	13.1	29.3	2.2
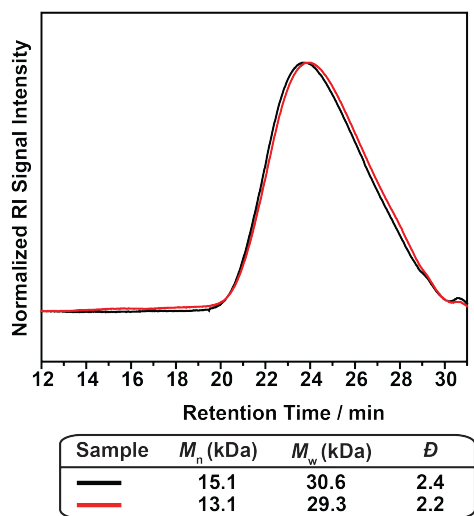
Figure S32. Styrene, **1**, CH_2Cl_2, 1 equiv. durene.

Sample	M_n (kDa)	M_w (kDa)	Đ
▬ (black)	64.3	127.2	1.9
▬ (red)	63.9	121.0	1.9
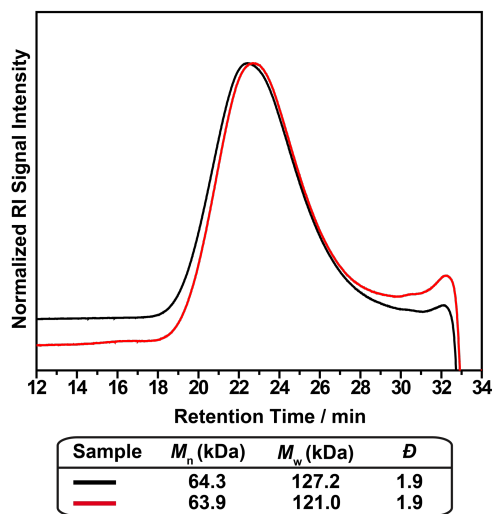
Figure S33. 4-bromostyrene, **1**, CH_2Cl_2, 1 equiv. durene.

Sample	M_n (kDa)	M_w (kDa)	Đ
——	12.1	30.1	2.5
——	12.9	33.6	2.6

Figure S34. Styrene, **3**, 1,2-difluorobenzene, 1 equiv. [NBu$_4$][**3**].
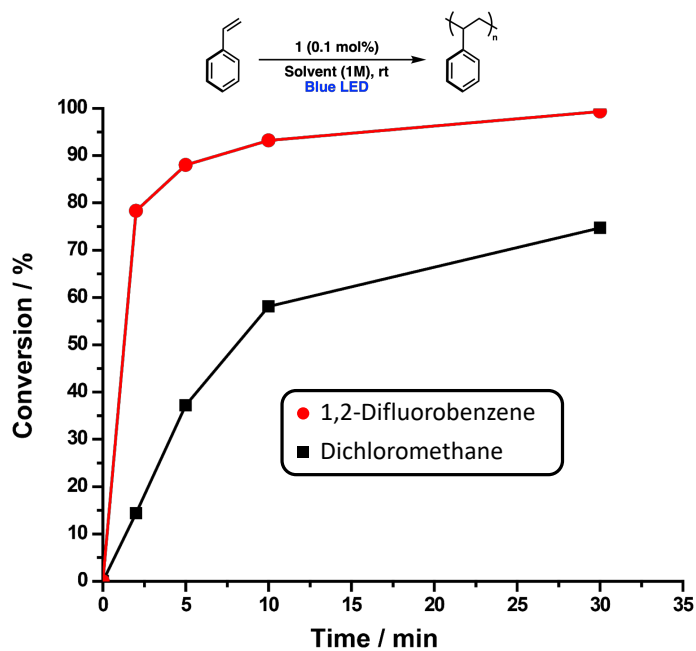
Figure S35. Rates of conversion of styrene in the presence of **1** in CH$_2$Cl$_2$ and 1,2-difluorobenzene. Aliquots were quenched with 50μL NEt$_3$/700μl CDCl$_3$. Hexamethyldisilane was used as an internal standard to measure conversion by ^{1}H NMR spectroscopy.
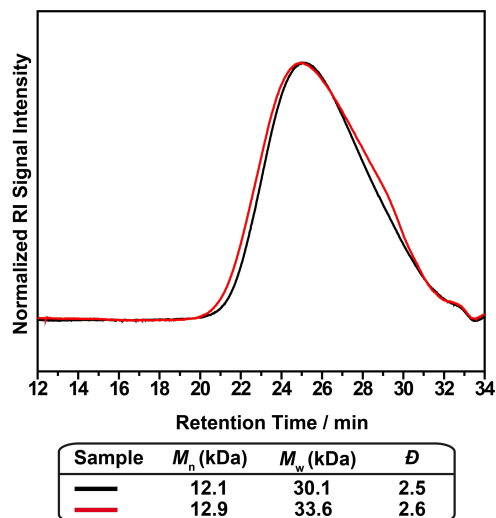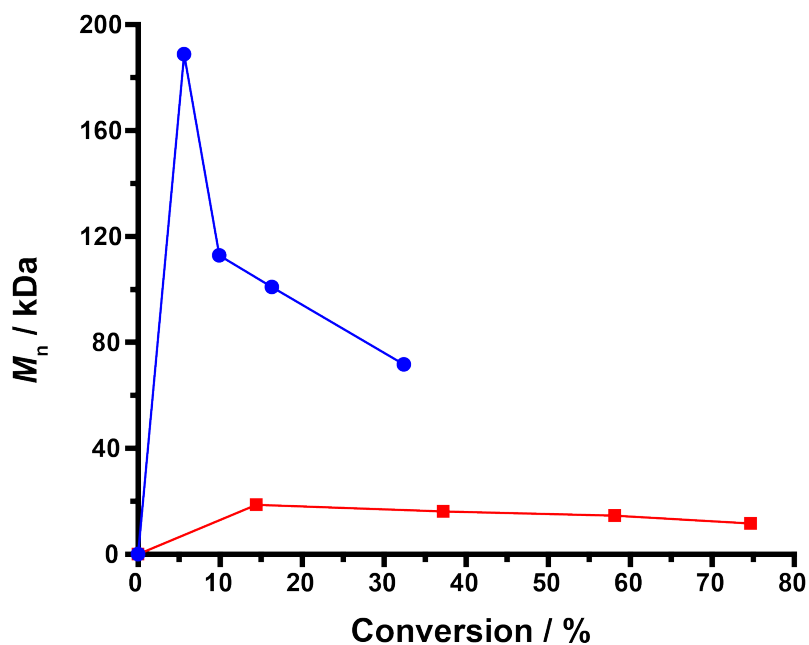
Figure S36. Timepoint analysis of the polymerization of S1 (red trace) and S4 (blue trace) initiated by **1** under standard reaction conditions.

Sample	M_n (kDa)	M_w (kDa)	Đ
——	97.6	274.4	2.8
——	103.9	354.8	3.4

Figure S37. GPC analysis of the polymerization of 2,4,6-trimethylstyrene initiated by **3** (0.1 mol%) in 1,2-difluorobenzene containing 0.1 mol% [NBu4][**3**] under standard conditions.

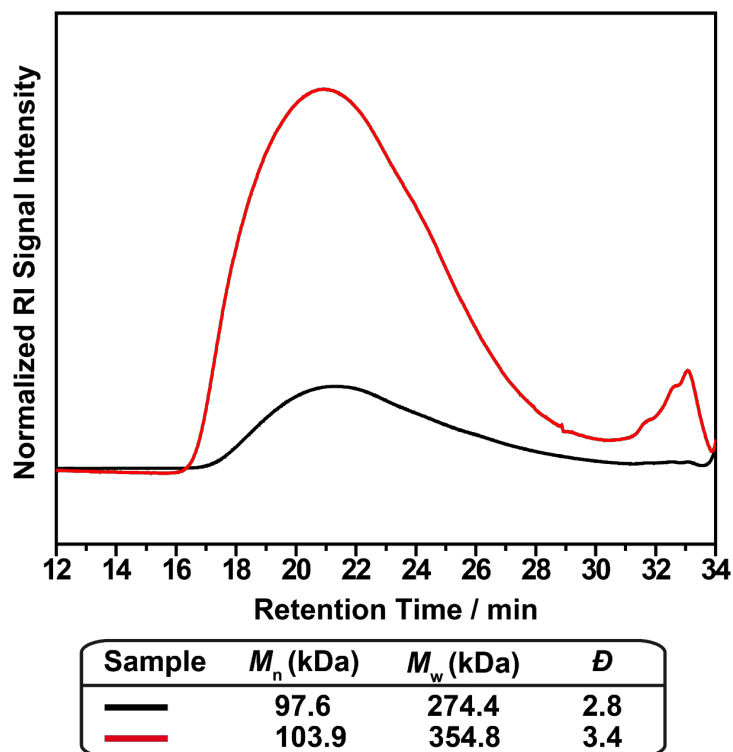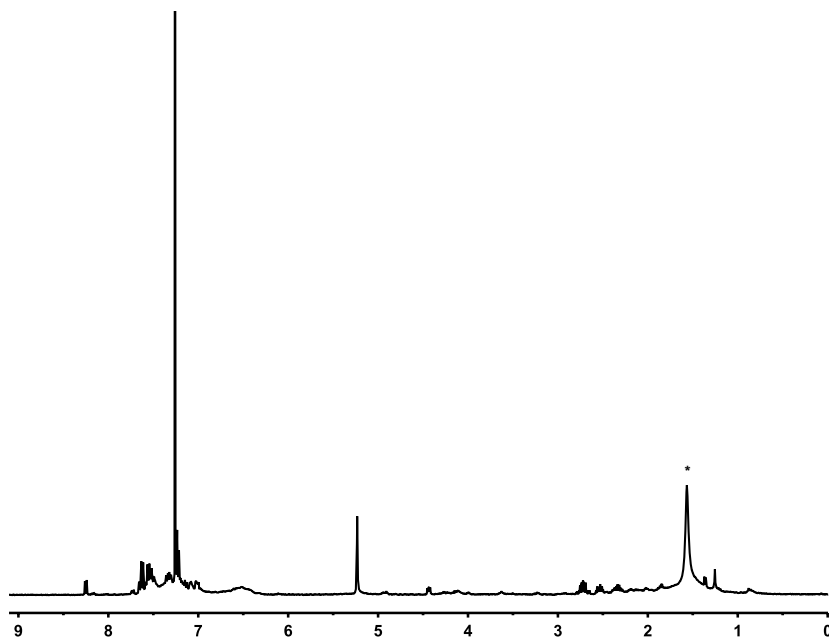**Figure S38**. ^{1}H NMR spectrum of the crude reaction mixture of **1** and 4-trifluoromethylstyrene in CDCl$_3$ after blue LED irradiation under standard conditions. Little to no oligomeric/polymeric products are observed. *Residual H$_2$O.

Representative MALDI data for polymerizations initiated by **1**, **2**, and **3**. Analysis was carried out primarily to determine if polymers were terminated with the initiators. There is no indication that the initiators remain on the polymer chain ends. The best spectrum resolution was obtained for analysis of poly(2-vinylnapthalene) and end-group analysis suggests polymers terminated with an alkene, -OMe, -OH, and –CH$_3$. These are plausible pathways given the likely presence of adventitious water, polymer precipitation from methanol, chain transfer due to water or deprotonation vicinal to the cationic chain end site.

Figure S39. 1, 2,4,6-trimethylstyrene, 1,2-difluorobenzene
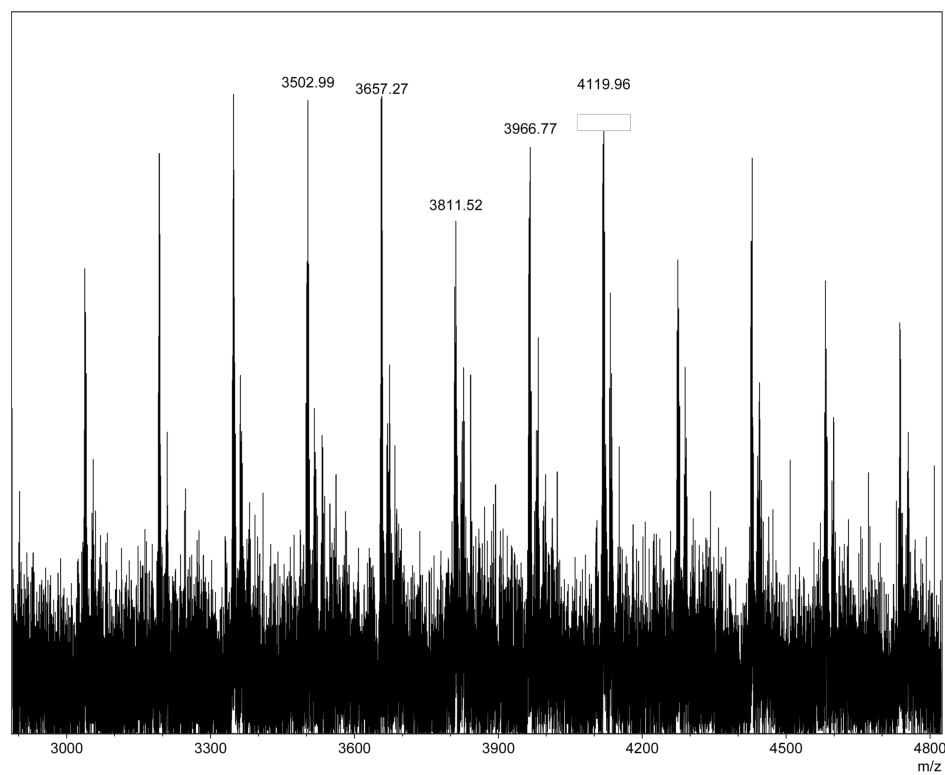
Figure S40. 2, 2-vinylnaphthalene, 1,2-difluorobenzene
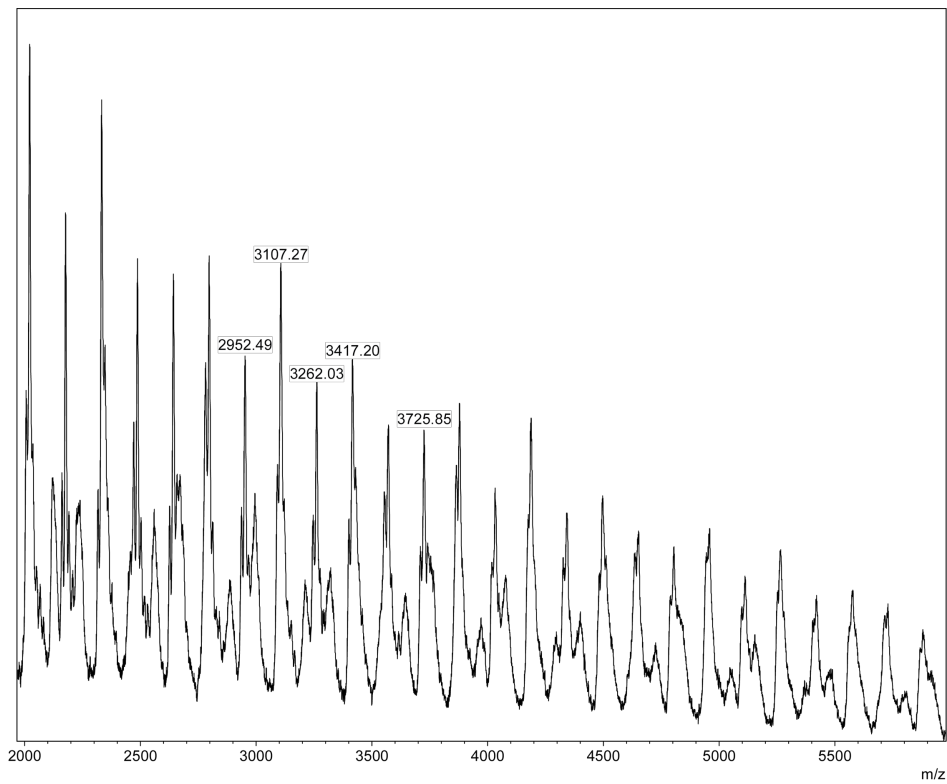
Figure S41. 3, 2-vinylnaphthalene, 1,2-difluorobenzene
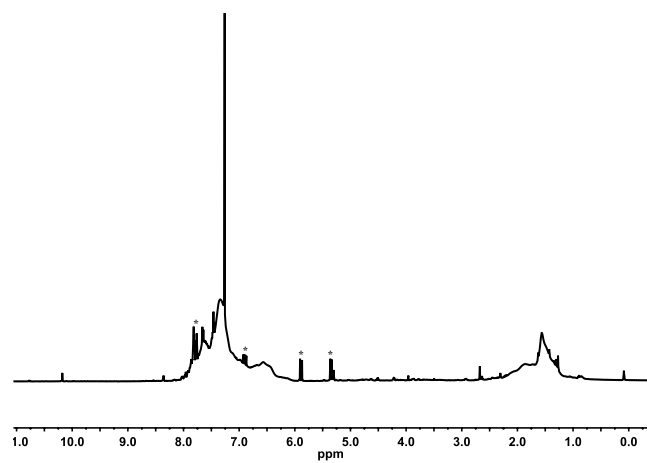
Figure S42. Representative ^{1}H NMR of poly-(2-vinylnaphthalene) in CDCl$_3$. * (residual monomer)
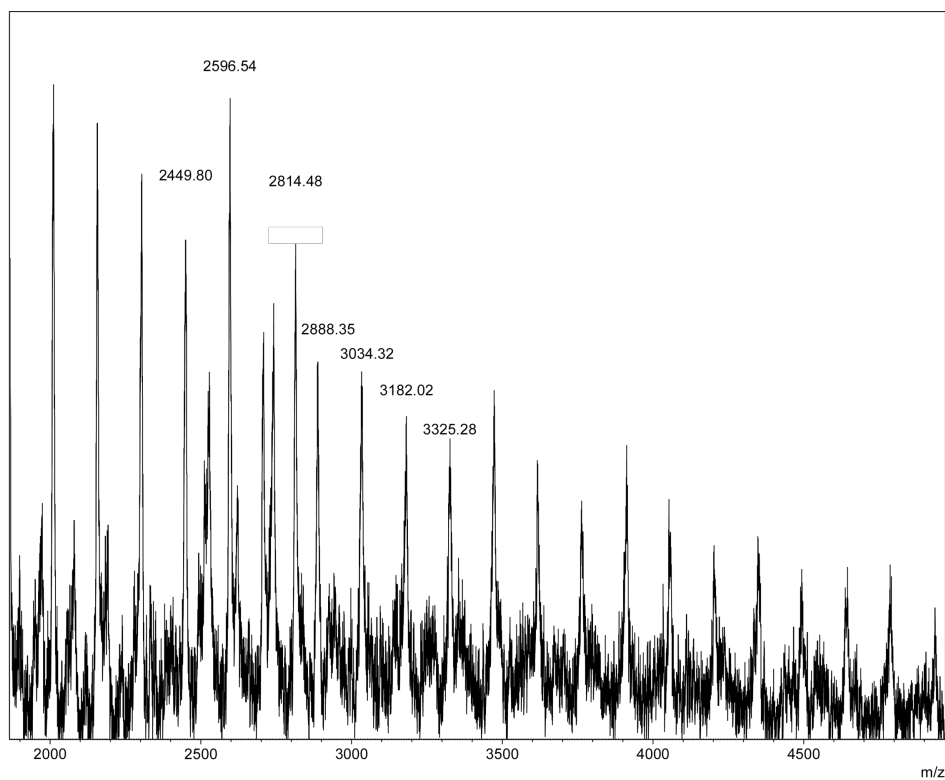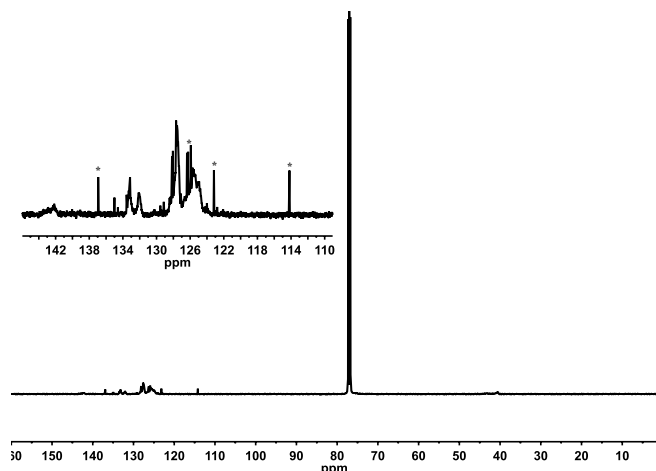
Figure S43. Representative ^{13}C NMR of poly (2-vinylnaphthalene) in CDCl₃. * (residual monomer)

Computational Details.

TD-DFT Simulations (Figure 3)

All the density functional theory (DFT) calculations were performed by Turbomole[5], using the τ-dependent gradient-corrected functional of Tao, Perdew, Staroverov, and Scuseria (TPSS)[6] with the def2-TZVP[7,8] basis set. All the time-dependent DFT(TD-DFT) results and molecular orbital energies were gained from Gaussian 09[9] program by using hybrid functional of TPSS(TPSSh)[6,10] with the cc-pvdz[11,12] basis set. Visualization for electronic and structural analysis (VESTA)[13][9] was also used for visualization.

Electronic transitions within **1**, **2**, and **3** investigated by the TD-DFT calculations showing the excited states and the corresponding molecular orbital energies.

Table S2. Electronic Excited States of **1**

Excited States No.	Excitation Energy/eV	Adsorption Wavelength/nm	Oscillator Strength	MO origin	Contribution of each MO
5	1.5638	792.84	0.0051	HOMO-4->LUMO	0.992
6	1.5722	788.59	0.0019	HOMO-5->LUMO	0.981
8	1.6309	760.22	0.0024	HOMO-7->LUMO	0.989
9	1.6353	758.19	0.0046	HOMO-8->LUMO	0.957

10	1.6608	746.55	0.0021	HOMO-9->LUMO	0.980
12	1.7332	715.33	0.0025	HOMO-11->LUMO	0.953
16	1.8219	680.51	0.0115	HOMO-21->LUMO	0.025
				HOMO-15->LUMO	0.884
19	1.9021	651.81	0.0080	HOMO-18->LUMO	0.983
20	1.9265	643.57	0.0018	HOMO-19->LUMO	0.974
22	2.0047	618.46	0.0017	HOMO-23->LUMO	0.045
				HOMO-22->LUMO	0.232
				HOMO-21->LUMO	0.662
23	2.0345	609.40	0.0153	HOMO-25->LUMO	0.041
				HOMO-22->LUMO	0.735
				HOMO-21->LUMO	0.181
25	2.1135	586.64	0.0017	HOMO-25->LUMO	0.128
				HOMO-24->LUMO	0.796
				HOMO-23->LUMO	0.039
26	2.1896	566.24	0.0082	HOMO-26->LUMO	0.444
				HOMO-25->LUMO	0.498
				HOMO-24->LUMO	0.027
27	2.2381	553.98	0.0012	HOMO-27->LUMO	0.953
				HOMO-26->LUMO	0.029
28	2.3733	522.41	0.0807	HOMO-29->LUMO	0.388
				HOMO-28->LUMO	0.222
				HOMO-26->LUMO	0.201

				HOMO-25->LUMO	0.096
				HOMO-21->LUMO	0.020
29	2.4338	509.42	0.0757	HOMO-29->LUMO	0.414
				HOMO-28->LUMO	0.539
30	2.5031	495.32	0.1628	HOMO-29->LUMO	0.163
				HOMO-28->LUMO	0.206
				HOMO-27->LUMO	0.021
				HOMO-26->LUMO	0.254
				HOMO-25->LUMO	0.159
				HOMO-24->LUMO	0.047
				HOMO-23->LUMO	0.029
				HOMO-21->LUMO	0.046
				HOMO-15->LUMO	0.028
31	2.7756	446.70	0.0115	HOMO-37->LUMO	0.034
				HOMO-30->LUMO	0.944
32	2.9055	426.72	0.0130	HOMO-36->LUMO	0.053
				HOMO-31->LUMO	0.916
33	3.0581	405.43	0.0010	HOMO-32->LUMO	0.977

Table S3. Energy of molecular orbitals in **1**

MOs	Energy/eV	MOs	Energy/eV	MOs	Energy/eV	MOs	Energy/eV
HOMO-42	-9.14	HOMO-30	-8.05	HOMO-18	-7.12	HOMO-6	-6.81

MO	Energy/eV	MO	Energy/eV	MO	Energy/eV	MO	Energy/eV
HOMO-41	-9.12	HOMO-29	-7.61	HOMO-17	-7.11	HOMO-5	-6.78
HOMO-40	-9.10	HOMO-28	-7.56	HOMO-16	-7.07	HOMO-4	-6.77
HOMO-39	-9.08	HOMO-27	-7.46	HOMO-15	-7.01	HOMO-3	-6.74
HOMO-38	-9.05	HOMO-26	-7.43	HOMO-14	-7.01	HOMO-2	-6.70
HOMO-37	-8.74	HOMO-25	-7.37	HOMO-13	-6.99	HOMO-1	-6.31
HOMO-36	-8.71	HOMO-24	-7.33	HOMO-12	-6.98	HOMO	-6.19
HOMO-35	-8.42	HOMO-23	-7.31	HOMO-11	-6.95	LUMO	-4.99
HOMO-34	-8.37	HOMO-22	-7.25	HOMO-10	-6.92	LUMO+1	-2.18
HOMO-33	-8.31	HOMO-21	-7.22	HOMO-9	-6.87		
HOMO-32	-8.23	HOMO-20	-7.16	HOMO-8	-6.85		
HOMO-31	-8.18	HOMO-19	-7.14	HOMO-7	-6.84		

Table S4. Excited States of **2**

Excited States No.	Excitation Energy/eV	Adsorption Wavelength/nm	Oscillator Strength	MO origin	Contribution of each MO
4	1.8825	658.62	0.0245	HOMO-4->LUMO	0.642
				HOMO-3->LUMO	0.348
5	1.9189	646.13	0.0490	HOMO-6->LUMO	0.052
				HOMO-4->LUMO	0.329
				HOMO-3->LUMO	0.565
6	1.9629	631.65	0.0096	HOMO-7->LUMO	0.032
				HOMO-5->LUMO	0.930
7	2.0076	617.57	0.0116	HOMO-7->LUMO	0.351
				HOMO-6->LUMO	0.579

				HOMO-5->LUMO	0.031
8	2.0283	611.27	0.0153	HOMO-7->LUMO	0.595
				HOMO-6->LUMO	0.318
9	2.0640	600.70	0.0020	HOMO-8->LUMO	0.991
10	2.1018	589.90	0.0018	HOMO-10->LUMO	0.053
				HOMO-9->LUMO	0.900
12	2.1296	582.21	0.0014	HOMO-11->LUMO	0.860
				HOMO-10->LUMO	0.126
13	2.1426	578.67	0.0060	HOMO-13->LUMO	0.101
				HOMO-12->LUMO	0.875
16	2.1838	567.74	0.0036	HOMO-15->LUMO	0.305
				HOMO-14->LUMO	0.670
17	2.2069	561.81	0.0015	HOMO-18->LUMO	0.061
				HOMO-17->LUMO	0.056
				HOMO-16->LUMO	0.753
				HOMO-15->LUMO	0.050
				HOMO-14->LUMO	0.036
19	2.2523	550.48	0.0101	HOMO-19->LUMO	0.726
				HOMO-18->LUMO	0.216
20	2.2551	549.79	0.0071	HOMO-22->LUMO	0.070
				HOMO-20->LUMO	0.111
				HOMO-19->LUMO	0.257
				HOMO-18->LUMO	0.490

21	2.2840	542.84	0.0021	HOMO-22->LUMO	0.122
				HOMO-21->LUMO	0.343
				HOMO-20->LUMO	0.469
				HOMO-18->LUMO	0.045
22	2.2886	541.74	0.0023	HOMO-22->LUMO	0.029
				HOMO-21->LUMO	0.640
				HOMO-20->LUMO	0.323
23	2.3381	530.29	0.0078	HOMO-26->LUMO	0.022
				HOMO-23->LUMO	0.699
				HOMO-22->LUMO	0.218
24	2.3584	525.70	0.0071	HOMO-28->LUMO	0.036
				HOMO-26->LUMO	0.077
				HOMO-24->LUMO	0.586
				HOMO-23->LUMO	0.089
				HOMO-22->LUMO	0.160
25	2.3914	518.46	0.0046	HOMO-25->LUMO	0.849
				HOMO-24->LUMO	0.075
				HOMO-23->LUMO	0.025
				HOMO-22->LUMO	0.024
26	2.4179	512.77	0.0113	HOMO-28->LUMO	0.150
				HOMO-27->LUMO	0.029
				HOMO-26->LUMO	0.714

				HOMO-25->LUMO	0.032
				HOMO-24->LUMO	0.058
28	2.4689	502.18	0.0930	HOMO-28->LUMO	0.450
				HOMO-27->LUMO	0.025
				HOMO-25->LUMO	0.076
				HOMO-24->LUMO	0.224
				HOMO-23->LUMO	0.102
				HOMO-22->LUMO	0.070
29	2.5296	490.14	0.0949	HOMO-29->LUMO	0.527
				HOMO-28->LUMO	0.099
				HOMO-26->LUMO	0.088
				HOMO-25->LUMO	0.023
				HOMO-24->LUMO	0.035
				HOMO-23->LUMO	0.023
				HOMO-22->LUMO	0.085
				HOMO-18->LUMO	0.027
30	2.6116	474.74	0.1162	HOMO-29->LUMO	0.430
				HOMO-28->LUMO	0.149
				HOMO-26->LUMO	0.050
				HOMO-23->LUMO	0.033
				HOMO-22->LUMO	0.151
				HOMO-18->LUMO	0.041
				HOMO-3->LUMO	0.024

				HOMO-37->LUMO	0.036
31	2.9497	420.33	0.0236	HOMO-37->LUMO	0.036
				HOMO-30->LUMO	0.929
32	3.0419	407.59	0.0401	HOMO-36->LUMO	0.068
				HOMO-31->LUMO	0.878
33	3.1796	389.93	0.0025	HOMO-35->LUMO	0.021
				HOMO-34->LUMO	0.047
				HOMO-33->LUMO	0.022
				HOMO-32->LUMO	0.880

Table S5. Energy of molecular orbitals in **2**

MOs	Energy/eV	MOs	Energy/eV	MOs	Energy/eV	MOs	Energy/eV
HOMO-37	-8.97	HOMO-27	-7.72	HOMO-17	-7.50	HOMO-7	-7.31
HOMO-36	-8.87	HOMO-26	-7.7	HOMO-16	-7.49	HOMO-6	-7.27
HOMO-35	-8.55	HOMO-25	-7.69	HOMO-15	-7.47	HOMO-5	-7.25
HOMO-34	-8.52	HOMO-24	-7.66	HOMO-14	-7.46	HOMO-4	-7.17
HOMO-33	-8.48	HOMO-23	-7.62	HOMO-13	-7.45	HOMO-3	-7.15
HOMO-32	-8.41	HOMO-22	-7.60	HOMO-12	-7.43	HOMO-2	-6.88
HOMO-31	-8.36	HOMO-21	-7.57	HOMO-11	-7.41	HOMO-1	-6.43
HOMO-30	-8.28	HOMO-20	-7.56	HOMO-10	-7.41	HOMO	-6.38
HOMO-29	-7.80	HOMO-19	-7.53	HOMO-9	-7.39	LUMO	-5.07
HOMO-28	-7.73	HOMO-18	-7.52	HOMO-8	-7.36		

Table S6. Excited States of **3**

Excited States No.	Excitation Energy/eV	Adsorption Wavelength/nm	Oscillator Strength	MO origin	Contribution of each MO
4	1.8577	667.41	0.0383	HOMO-3->LUMO	0.989
6	1.9587	632.98	0.0465	HOMO-6->LUMO	0.151
				HOMO-5->LUMO	0.036
				HOMO-4->LUMO	0.801
7	2.0324	610.03	0.0260	HOMO-12->LUMO	0.033
				HOMO-11->LUMO	0.073
				HOMO-6->LUMO	0.758
				HOMO-4->LUMO	0.113
10	2.1228	584.07	0.0016	HOMO-10->LUMO	0.191
				HOMO-9->LUMO	0.388
				HOMO-8->LUMO	0.416
12	2.1876	566.76	0.0074	HOMO-12->LUMO	0.570
				HOMO-11->LUMO	0.420
13	2.2056	562.12	0.0011	HOMO-13->LUMO	0.967
16	2.3025	538.48	0.0314	HOMO-25->LUMO	0.024
				HOMO-22->LUMO	0.137
				HOMO-20->LUMO	0.048
				HOMO-16->LUMO	0.185
				HOMO-12->LUMO	0.208
				HOMO-11->LUMO	0.289
				HOMO-6->LUMO	0.025

17	2.3061	537.64	0.0158	HOMO-22->LUMO	0.048
				HOMO-16->LUMO	0.799
				HOMO-12->LUMO	0.051
				HOMO-11->LUMO	0.047
18	2.3176	534.97	0.0013	HOMO-17->LUMO	0.962
19	2.3498	527.64	0.0178	HOMO-23->LUMO	0.035
				HOMO-22->LUMO	0.028
				HOMO-18->LUMO	0.894
22	2.3821	520.49	0.0050	HOMO-23->LUMO	0.102
				HOMO-22->LUMO	0.069
				HOMO-21->LUMO	0.096
				HOMO-20->LUMO	0.702
24	2.4326	509.69	0.0015	HOMO-25->LUMO	0.775
				HOMO-24->LUMO	0.022
				HOMO-23->LUMO	0.046
				HOMO-22->LUMO	0.143

25	2.4387	508.4	0.0486	HOMO-27->LUMO	0.044
				HOMO-24->LUMO	0.033
				HOMO-23->LUMO	0.444
				HOMO-22->LUMO	0.242
				HOMO-20->LUMO	0.123
				HOMO-12->LUMO	0.024
				HOMO-11->LUMO	0.046
27	2.5033	495.28	0.0326	HOMO-29->LUMO	0.042
				HOMO-27->LUMO	0.642
				HOMO-25->LUMO	0.050
				HOMO-23->LUMO	0.148
				HOMO-22->LUMO	0.057
28	2.5159	492.81	0.0050	HOMO-28->LUMO	0.877
				HOMO-27->LUMO	0.068
29	2.5791	480.73	0.0944	HOMO-29->LUMO	0.133
				HOMO-28->LUMO	0.098
				HOMO-27->LUMO	0.230
				HOMO-25->LUMO	0.077
				HOMO-23->LUMO	0.058
				HOMO-22->LUMO	0.166
				HOMO-18->LUMO	0.032
				HOMO-12->LUMO	0.063
				HOMO-11->LUMO	0.067
				HOMO-6->LUMO	0.031
30	2.6246	472.39	0.0804	HOMO-29->LUMO	0.796
				HOMO-25->LUMO	0.023
				HOMO-23->LUMO	0.053
				HOMO-22->LUMO	0.049
31	2.9317	422.91	0.0258	HOMO-37->LUMO	0.037
				HOMO-31->LUMO	0.051
				HOMO-30->LUMO	0.877
32	3.0001	413.27	0.0233	HOMO-36->LUMO	0.088
				HOMO-35->LUMO	0.033
				HOMO-31->LUMO	0.805
				HOMO-30->LUMO	0.051

Table S7. Energy of molecular orbitals in **3**

MOs	Energy/eV	MOs	Energy/eV	MOs	Energy/eV	MOs	Energy/eV
HOMO-41	-9.64	HOMO-30	-8.66	HOMO-19	-8.05	HOMO-8	-7.80
HOMO-40	-9.61	HOMO-29	-8.28	HOMO-18	-8.04	HOMO-7	-7.75
HOMO-39	-9.57	HOMO-28	-8.22	HOMO-17	-8.01	HOMO-6	-7.68
HOMO-38	-9.45	HOMO-27	-8.21	HOMO-16	-8.00	HOMO-5	-7.63
HOMO-37	-9.33	HOMO-26	-8.16	HOMO-15	-7.95	HOMO-4	-7.62
HOMO-36	-9.16	HOMO-25	-8.14	HOMO-14	-7.94	HOMO-3	-7.53
HOMO-35	-8.96	HOMO-24	-8.12	HOMO-13	-7.92	HOMO-2	-7.26
HOMO-34	-8.96	HOMO-23	-8.11	HOMO-12	-7.90	HOMO-1	-6.78
HOMO-33	-8.82	HOMO-22	-8.11	HOMO-11	-7.89	HOMO	-6.77
HOMO-32	-8.81	HOMO-21	-8.08	HOMO-10	-7.83	LUMO	-5.48
HOMO-31	-8.75	HOMO-20	-8.08	HOMO-9	-7.81		

Table S8. Ionization energies of styrene, 4-methylstyrene, 4-chlorostyrene, and 2,4,6-trimethylstyrene.

	Gas/eV		Solution@CH_2Cl_2/eV	
	Vertical	Adiabatic	Vertical	Adiabatic
Styrene	8.12	7.99	6.33	6.21
4-CH3-Styrene	7.82	7.69	6.14	6.01
4-Cl-Styrene	8.02	7.89	6.30	6.16
2,4,6-Me_3-Styrene	7.66	7.48	5.98	5.90

Table S9. Electron Affinities of pentafluorobenzene, 1,3-bis(trifluoromethyl)benzene, and benzotrifluoride

	Gas/eV		Liquid/eV	
	Vertical	Adiabatic	Vertical	Adiabatic

Pentafluorobenzene	-0.95	0.13	0.89	1.98
1,3-$(CF_3)_2$-C_6H_4	-0.39	0.26	1.35	1.93
Benzotrifluoride	-0.79	-0.41	1.20	1.59

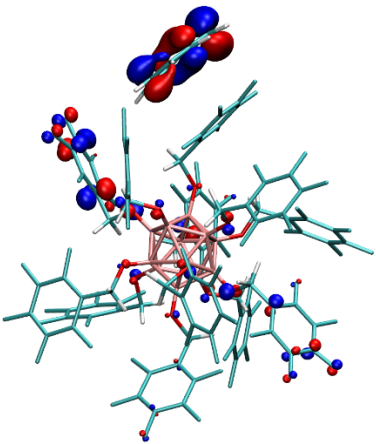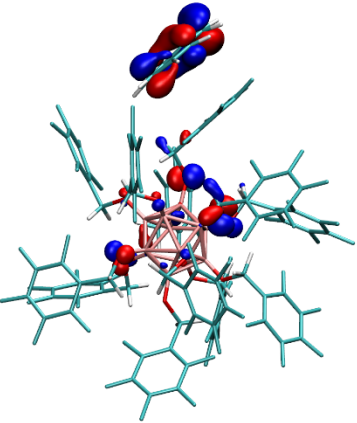**Theoretical Modeling of the Systems** (Figure 5 in the text).

The studied systems were modeled by classical and quantum molecular dynamics simulations and *ab initio* electronic structure methods. In order to find proper positions of molecules for molecular orbital overlap studies, resulting in the electron transfer between **1 – 3** and styrene, classical atomistic molecular dynamic simulations (MD) were performed of the frozen optimized dodecaborane cluster **1** (B3LYP/6-31gs) and 3 styrene molecules in an explicit solvent (CH_2Cl_2 and CH_3CN). The classical MD simulations were performed with NAMD[14] in an NPT ensemble with P = 1 bar and T = 300 K, using a Langevin dynamics with a damping constant of 1 ps^{-1} and a time step of 2 fs. Nonbonding interactions were calculated using a cutoff distance of 10 Å and long-range electrostatic interactions were calculated using the PME method[15] in the presence of periodic boundary conditions. Molecular force field parameters were obtained from the CHARMM general force field.[16,17] *Ab Initio* molecular dynamic simulations were performed using an NVT ensemble at T=300 K using a Langevin thermostat and a time step of 0.5 fs. A polarizable continuum model (PCM) ($\varepsilon(CH_2Cl_2)$ = 8.93, $\varepsilon(CH_3CN)$ = 36.64) and hybrid (molecules within 8 Å of dodecaborane cluster **1** are treated explicitly placed within implicit shell of the solvent) solvation were implemented. After classical MD simulations, a sphere of a radius 8 Å was cut around the cluster, including one styrene molecule in a co-facial interaction with one cluster ligand and several solvent molecules around it. Electronic absorption spectra were calculated to access the energies of the molecular orbitals (MOs). The time-dependent DFT (TD-DFT)/B3LYP method with 6-31g* basis set was used for the calculation of the excited states energies. The quantum chemical calculations used in this analysis were performed with TERAChem[18] and visualization was done with VMD[19].

Supplementary Movie 1 | Atomistic molecular dynamics simulation of dodecaborane **1** and 3 styrene residues at room temperature in explicit CH_3CN (deleted for clarity). The movie is attached separately.

Supplementary Movie 2 | Atomistic molecular dynamics simulation of dodecaborane **1** and 3 styrene residues at room temperature in explicit CH_2Cl_2 (deleted for clarity). The movie is attached separately.
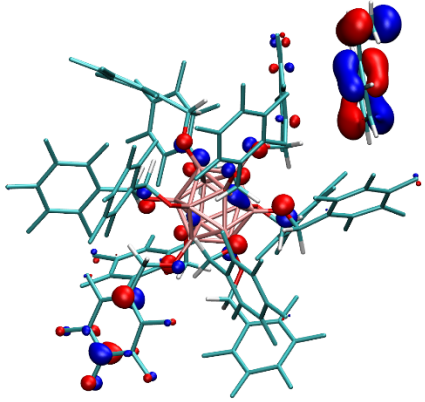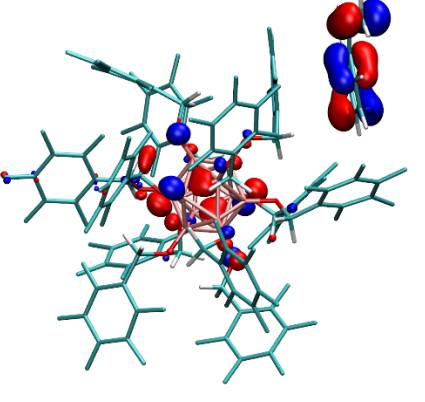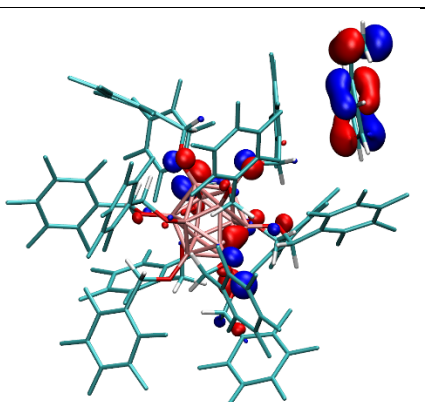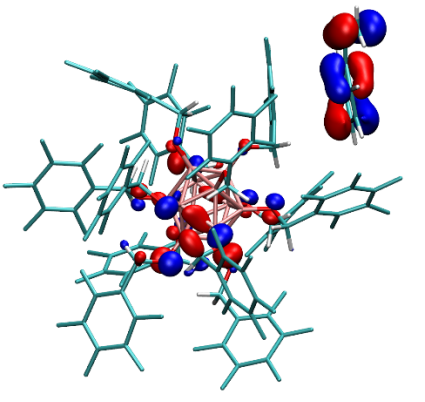
Electronic spectra were calculated by a TD-DFT method, as described above. Some important features are shown for the transitions with a transition dipole moment larger than 1 (see below). All the studied transitions go to LUMO. In the case of CH_3CN, only a small overlap in the co-facial position between dodecaborane **1** and styrene was observed. On the other hand, calculations in CH_2Cl_2 resulted in a strong overlap for the co-facial and edge-on positions. These interactions could be the key for proposed mechanism and result in more efficient electron transfer and polymerization initiation.

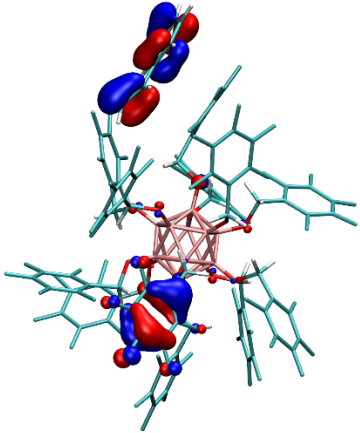**Table S10.** Character of Excited states
CH₃CN PCM (Snapshot 2141)

Wavelength, nm	Excitation Energy, eV	Oscillator strength, f	Molecular Orbitals	Representation
410	3.02	0.1592	HOMO-27	
397	3.11	0.0937	HOMO-29	
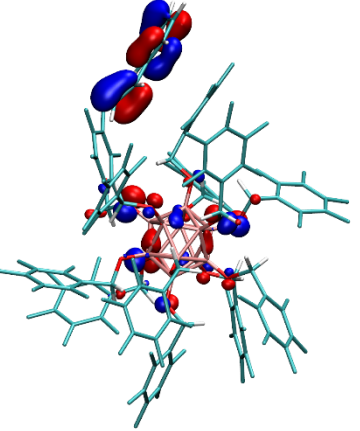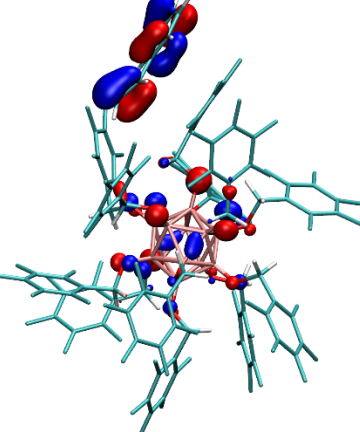
CH₃CN Hybrid (Snapshot 2141)
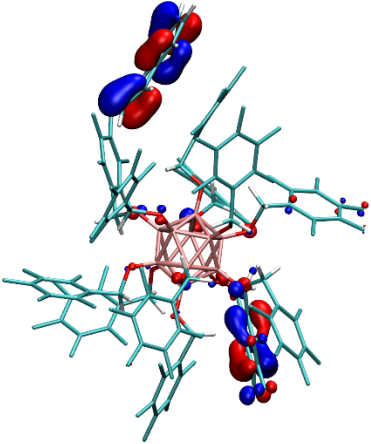
Wavelength, nm	Excitation Energy, eV	Oscillator strength, f	Molecular Orbitals	Representation

457	2.71	0.1233	HOMO-27	
420	2.95	0.2168	HOMO-28	
409	3.03	0.1074	HOMO-29	
383	3.23	0.0800	HOMO-30	
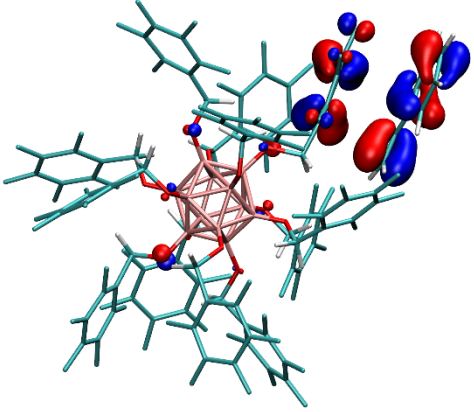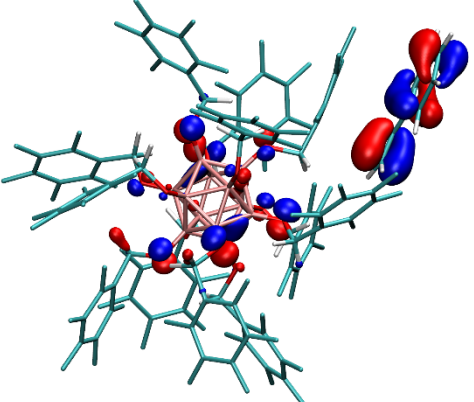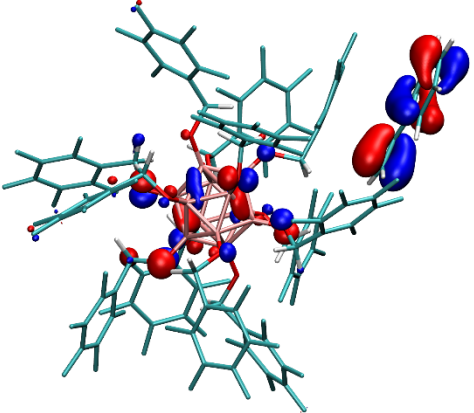
CH$_2$Cl$_2$ PCM (Snapshot 43)

Wavelength, nm	Excitation Energy, eV	Oscillator strength, f	Molecular Orbitals	Representation
460	2.69	0.1588	HOMO-27	
443	2.79	0.0876	HOMO-29	
432	2.86	0.0565	HOMO-30	
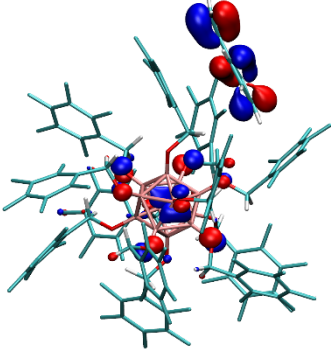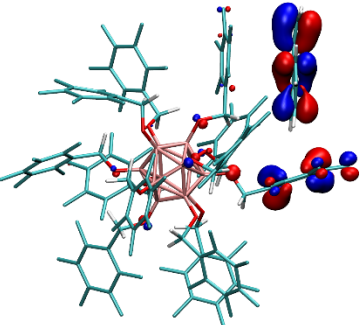
425	2.91	0.1795	HOMO-28	
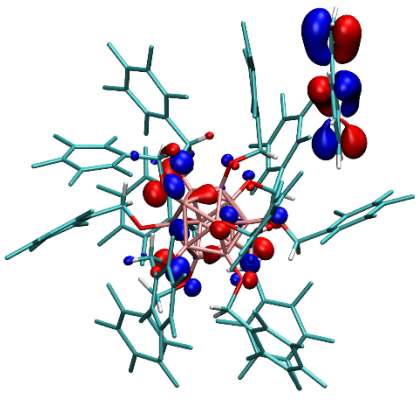
CH$_2$Cl$_2$ Hybrid (Snapshot 43)

Wavelength, nm	Excitation Energy, eV	Oscillator strength, f	Molecular Orbitals	Representation
465	2.66	0.1049	HOMO-27	
430	2.88	0.0733	HOMO-29	
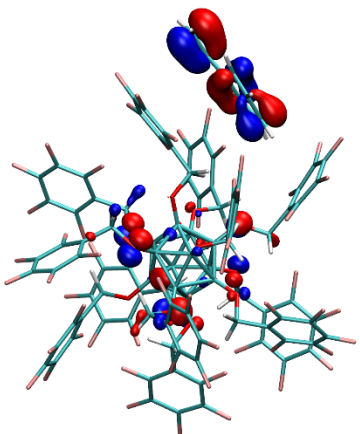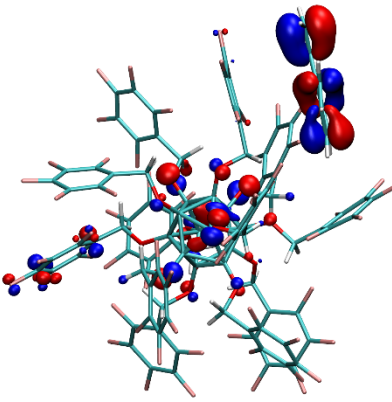
422	2.93	0.2687	HOMO-28	
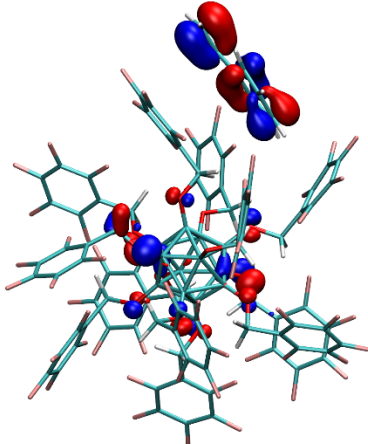
CH$_2$Cl$_2$ PCM (Snapshot 2705)

Wavelength, nm	Excitation Energy, eV	Oscillator strength, f	Molecular Orbitals	Representation
444	2.79	0.1450	HOMO-28	
426	2.91	0.2000	HOMO-27	

416	3.01	0.1386	HOMO-29	

CH$_2$Cl$_2$ Hybrid (Snapshot 2705)

Wavelength, nm	Excitation Energy, eV	Oscillator strength, f	Molecular Orbitals	Representation
438	2.83	0.0875	HOMO-29	
432	2.86	0.1401	HOMO-28	

409	3.02	0.1007	HOMO-30	

Emission Spectroscopy.

Steady-state fluorescence was measured in perfluorotoluene glass at 77K. Samples were prepared in quartz spectroscopy tubes (ID = 3 mm, OD = 4 mm) under argon atmosphere and rapidly frozen by immersion of the sample tube in liquid nitrogen. A 457.9 nm excitation source (Coherent Innova 70 argon-ion laser) was directed at a quartz immersion Dewar containing the sample. Luminescence was passed to a Melles Griot 13 FOS 200 Spectrometer through an optical fiber. A 457.9 nm long-pass cutoff filter was used to exclude excitation light.
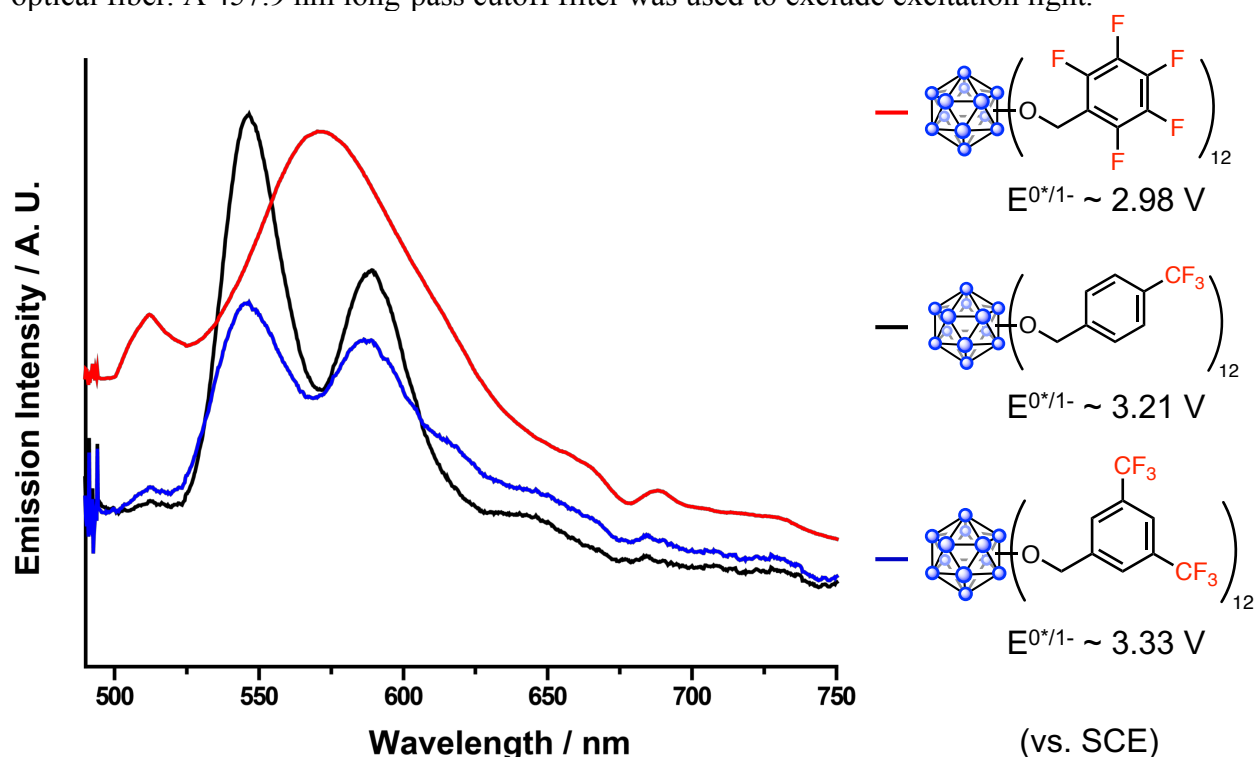

Figure S44. Emission data collected for **1 – 3** in C_7F_8 at 77K.

The reduction potentials of photo-excited **1 – 3** were approximated[20] using in Eq. 1,

$$E_{red}^{*}{}^{0} = E_{red}{}^{0} + E_{0,0} \tag{1}$$

where $E_{red}{}^{0}$ represents the ground state 0/1- redox couple of and $E_{0,0}$ represents the wavelength of the onset of fluorescence. Redox values are initially calculated based on the Fc/Fc^{+} reference and converted to SCE based on values reported by Connelly and Geiger,[21] where the formal potential of Fc/Fc^{+} referenced to SCE in CH$_3$CN with [NBu$_4$][PF$_6$] as the supporting electrolyte is 0.40 V.

Extinction Coefficient Measurements.

Absorption Spectra of 2 in CH$_2$Cl$_2$

ε = 19,890 M^{-1}cm^{-1}

y = 19890x + 0.0188
R² = 0.9997
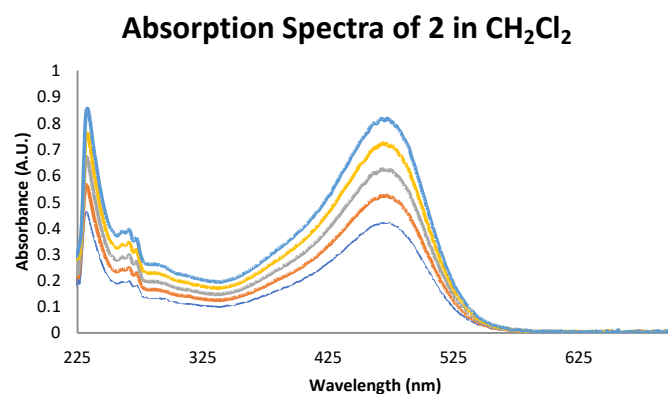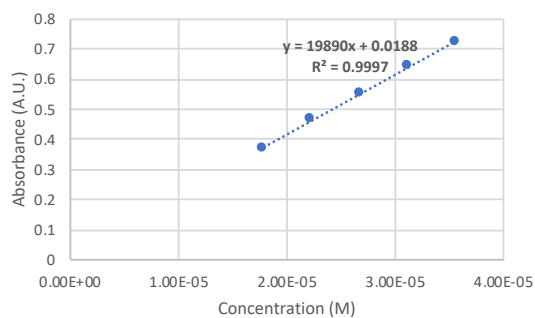
λ = 450.0635

Concentration (M)	Absorbance (A.U.)
1.79E-05	0.3721
2.23E-05	0.4642
2.68E-05	0.5542
3.13E-05	0.6425
3.57E-05	0.7265

Absorption Spectra of 3 in CH$_2$Cl$_2$

ε = 18,167 M^{-1}cm^{-1}

y = 18167x - 0.0119
R² = 0.9997
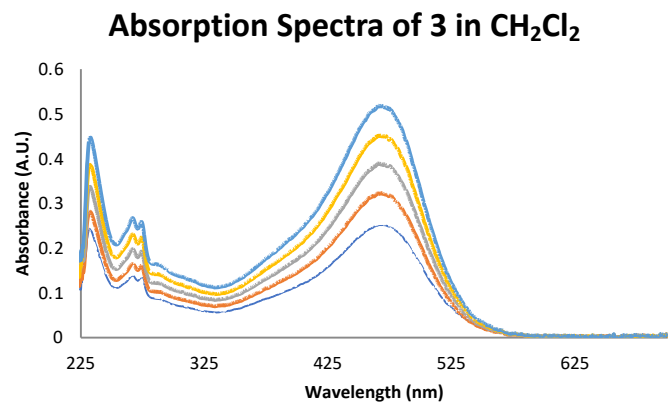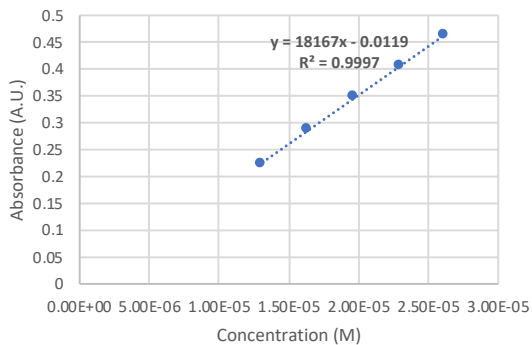
λ = 450.0635 nm

Concentration (M)	Absorbance (A.U.)
1.31E-05	0.2244
1.64E-05	0.2884
1.97E-05	0.3468
2.30E-05	0.4043
2.62E-05	0.4644

Crystallographic Information

Table 1. Crystal data and structure refinement for **3**.

Empirical formula	C108 H60 B12 F72 O12
Formula weight	3047.28
Temperature	100.0 K
Wavelength	0.71073 Å
Crystal system	Triclinic
Space group	P-1
Unit cell dimensions	a = 14.1766(8) Å α= 68.715(2)°.
	b = 14.8867(9) Å β= 86.112(2)°.
	c = 15.5797(10) Å γ = 76.641(2)°.
Volume	2980.3(3) Å^3
Z	1
Density (calculated)	1.698 Mg/m^3
Absorption coefficient	0.183 mm^{-1}
F(000)	1512
Crystal size	0.3 x 0.3 x 0.1 mm^3
Theta range for data collection	1.403 to 28.321°.
Index ranges	-18<=h<=18, -19<=k<=19, -20<=l<=18
Reflections collected	52159
Independent reflections	14805 [R(int) = 0.0483]
Completeness to theta = 25.242°	100.0 %
Absorption correction	Semi-empirical from equivalents
Max. and min. transmission	0.0962 and 0.0626
Refinement method	Full-matrix least-squares on F^2
Data / restraints / parameters	14805 / 0 / 947
Goodness-of-fit on F^2	1.051
Final R indices [I>2sigma(I)]	R1 = 0.0550, wR2 = 0.1414
R indices (all data)	R1 = 0.0701, wR2 = 0.1556
Extinction coefficient	n/a
Largest diff. peak and hole	1.268 and -0.885 e.Å^{-3}

Table 2. Atomic coordinates (x 10^4) and equivalent isotropic displacement parameters (Å^{2}x 10^3) for **3**. U(eq) is defined as one third of the trace of the orthogonalized U^{ij} tensor.

	x	y	z	U(eq)
F(1)	3165(1)	29(1)	7396(1)	45(1)
F(2)	3506(1)	750(1)	8265(1)	42(1)
F(3)	2114(1)	364(1)	8358(1)	54(1)
F(4)	231(2)	3805(2)	7624(1)	79(1)
F(5)	-429(1)	3830(2)	6461(2)	96(1)
F(6)	402(2)	4878(1)	6369(2)	97(1)
F(7)	2723(1)	9081(1)	6041(1)	45(1)
F(8)	2637(1)	7979(1)	7354(1)	43(1)
F(9)	1533(1)	9322(1)	6922(1)	56(1)

F(10)	-1477(1)	7566(2)	5978(2)	68(1)
F(11)	-1440(1)	9009(3)	5929(3)	150(2)
F(12)	-1329(1)	8661(2)	4702(2)	81(1)
F(13)	196(1)	7311(2)	508(2)	116(1)
F(14)	395(2)	8693(3)	408(3)	171(2)
F(15)	641(1)	8241(2)	-728(1)	69(1)
F(16)	4265(2)	7743(2)	-1152(1)	76(1)
F(17)	4118(2)	6291(2)	-906(1)	77(1)
F(18)	5121(1)	6543(2)	-106(1)	91(1)
F(19)	8107(1)	8600(1)	-94(1)	36(1)
F(20)	7124(1)	8282(1)	-882(1)	37(1)
F(21)	8655(1)	7709(1)	-921(1)	41(1)
F(22)	9493(1)	4215(1)	721(1)	42(1)
F(23)	9375(1)	3805(1)	2186(1)	47(1)
F(24)	8290(1)	3618(1)	1422(1)	54(1)
F(25)	9399(1)	1590(2)	7152(2)	79(1)
F(26)	9363(1)	589(1)	6506(1)	54(1)
F(27)	9578(1)	64(2)	7952(2)	134(2)
F(28)	6816(1)	770(1)	9936(1)	40(1)
F(29)	5976(1)	-130(1)	9656(1)	36(1)
F(30)	5388(1)	1426(1)	9318(1)	35(1)
F(31)	1672(1)	4813(1)	2343(1)	56(1)
F(32)	2164(1)	4985(1)	972(1)	55(1)
F(33)	1413(1)	3833(1)	1693(1)	55(1)
F(34)	4855(8)	459(6)	3050(20)	196(12)
F(34')	4498(4)	593(4)	2458(3)	65(1)
F(35)	3996(13)	604(5)	4177(6)	121(6)
F(35')	4897(4)	415(3)	3787(3)	69(2)
F(36)	3328(9)	689(7)	3004(8)	79(3)
F(36')	3424(3)	555(4)	3470(6)	87(3)
O(1)	2984(1)	6485(1)	4729(1)	19(1)
O(2)	4151(1)	5974(1)	2974(1)	19(1)
O(3)	6470(1)	5509(1)	3391(1)	20(1)
O(4)	5464(1)	3600(1)	3874(1)	20(1)
O(5)	4977(1)	2744(1)	5997(1)	20(1)
O(6)	3221(1)	4338(1)	4549(1)	20(1)
C(1)	3149(1)	3331(1)	4725(1)	22(1)

C(2)	2596(1)	2966(1)	5601(1)	22(1)
C(3)	2910(2)	2027(2)	6247(1)	25(1)
C(4)	2390(2)	1706(2)	7054(1)	27(1)
C(5)	1566(2)	2318(2)	7229(1)	28(1)
C(6)	1254(2)	3263(2)	6573(1)	27(1)
C(7)	1758(1)	3582(2)	5763(1)	24(1)
C(8)	2784(2)	706(2)	7771(2)	33(1)
C(9)	364(2)	3945(2)	6743(2)	34(1)
C(10)	2086(1)	6231(1)	5089(1)	21(1)
C(11)	1534(1)	7007(1)	5455(1)	20(1)
C(12)	2028(1)	7444(1)	5881(1)	22(1)
C(13)	1521(1)	8168(2)	6210(1)	24(1)
C(14)	519(2)	8462(2)	6129(2)	29(1)
C(15)	32(2)	8018(2)	5711(2)	31(1)
C(16)	529(1)	7298(2)	5373(1)	25(1)
C(17)	2088(2)	8645(2)	6633(2)	29(1)
C(18)	-1053(2)	8328(2)	5592(2)	50(1)
C(19)	3133(1)	6383(1)	2775(1)	20(1)
C(20)	2949(1)	6737(1)	1753(1)	20(1)
C(21)	3683(2)	6655(2)	1130(1)	24(1)
C(22)	3462(2)	6984(2)	194(1)	30(1)
C(23)	2517(2)	7410(2)	-135(2)	33(1)
C(24)	1790(2)	7493(2)	488(2)	30(1)
C(25)	1996(2)	7162(2)	1426(1)	26(1)
C(26)	4248(2)	6885(2)	-480(2)	43(1)
C(27)	754(2)	7948(2)	166(2)	47(1)
C(28)	6319(1)	6398(1)	2594(1)	21(1)
C(29)	7054(1)	6267(1)	1876(1)	20(1)
C(30)	7615(1)	5344(1)	1957(1)	21(1)
C(31)	8285(1)	5243(1)	1282(1)	23(1)
C(32)	8410(1)	6060(2)	524(1)	24(1)
C(33)	7842(1)	6982(2)	447(1)	24(1)
C(34)	7165(1)	7089(1)	1114(1)	22(1)
C(35)	8866(2)	4226(2)	1394(2)	30(1)
C(36)	7940(2)	7888(2)	-364(1)	28(1)
C(37)	5717(1)	1940(1)	5914(1)	22(1)
C(38)	6399(1)	1517(1)	6737(1)	22(1)

C(39)	7397(2)	1298(1)	6636(1)	25(1)
C(40)	8010(2)	922(1)	7406(1)	26(1)
C(41)	7639(2)	751(1)	8284(1)	26(1)
C(42)	6637(2)	961(1)	8384(1)	24(1)
C(43)	6018(1)	1342(1)	7619(1)	23(1)
C(44)	6208(2)	754(2)	9326(1)	29(1)
C(45)	9087(2)	754(2)	7274(2)	38(1)
C(46)	5426(1)	3875(1)	2884(1)	21(1)
C(47)	4637(1)	3444(1)	2691(1)	21(1)
C(48)	3762(1)	4040(2)	2294(1)	23(1)
C(49)	3011(2)	3622(2)	2189(1)	28(1)
C(50)	3131(2)	2609(2)	2476(2)	31(1)
C(51)	4014(2)	2011(2)	2872(2)	32(1)
C(52)	4766(2)	2418(2)	2979(1)	27(1)
C(53)	2065(2)	4304(2)	1799(2)	40(1)
C(54)	4169(2)	904(2)	3182(3)	54(1)
B(1)	3853(1)	5784(2)	4834(1)	17(1)
B(2)	4512(2)	5590(2)	3871(1)	17(1)
B(3)	5768(2)	5326(2)	4062(1)	18(1)
B(4)	5262(1)	4247(2)	4338(1)	18(1)
B(5)	4006(2)	4579(2)	4809(1)	18(1)
B(6)	5030(1)	3736(2)	5528(1)	17(1)

[1] a) Farha, O. K.; Julius, R. L.; Lee, M. W.; Huertas, R. E.; Knobler, C. B.; Hawthorne, M. F. Synthesis of Stable Dodecaalkoxy Derivatives of *hypercloso*-$B_{12}H_{12}$. *J. Am. Chem. Soc.* **2005**, *127*, 18243-18251; b) Bayer, M. J.; Hawthorne, M. F. An Improved Method for the Synthesis of [*closo*-$B_{12}(OH)_{12}]^{-2}$. *Inorg. Chem.* **2004**, *43*, 2018-2020.

[2] Messina, M. S.; Axtell, J. C.; Wang, Y.; Chong, P.; Wixtrom, A. I.; Kirlikovali, K. O.; Upton, B. M.; Hunter, B. M.; Shafaat, O. S.; Khan, S. I.; Winkler, J. R.; Gray, H. B.; Alexandrova, A. N.; Maynard, H. D.; Spokoyny, A. M. Visible-Light-Induced Olefin Activation Using 3D Aromatic Boron-Rich Cluster Photooxidants. *J. Am. Chem. Soc.* **2016**, *138*, 6952-6955.

[3] Wixtrom, A. I.; Shao, Y.; Jung, D.; Machan, C. W.; Kevork, S. N.; Qian, E. A.; Axtell, J. C.; Khan, S. I.; Kubiak, C. P.; Spokoyny, A. M. Rapid Synthesis of Redox-Active Dodecaborane $B_{12}(OR)_{12}$ Clusters Under Ambient Conditions. *Inorg. Chem. Front.* **2016**, *3,* 711-717.

[4] Aubry, T. J.; Axtell, J. C.; Basile, V. M.; Winchell, K. J.; Lindemuth, J. R.; Porter, T. M.; Liu, J.-Y.; Alexandrova, A. N.; Kubiak, C. P.; Tolbert, S. H.; Spokoyny, A. M.; Schwartz, B. J. Dodecaborane-Based Dopants Designed to Shield Anion Electrostatics Lead to Increased Carrier Mobility in a Doped Conjugated Polymer. *Adv. Mater.* **2019**, *31*, 1805647.

[5] TURBOMOLE V6.6 2014, a development of University of Karlsruhe and Forschungszentrum Karlsruhe GmbH, 1989-2007, TURBOMOLE GmbH, since 2007; available from http://www.turbomole.com.

[6] Tao, J. M.; Perdew, J. P.; Staroverov, V. N.; Scuseria, G. E. Climbing the Density Functional Ladder: Nonempirical Meta–Generalized Gradient Approximation Designed for Molecules and Solids. *Phys. Rev. Lett.* **2003**, *91*, 146401.

[7] Weigend, F.; Ahlrichs, R. Balanced Basis Sets of Split Valence, Triple Zeta Valence and Quadruple Zeta Valence Quality for H to Rn: Design and Assessment of Accuracy. *Phys. Chem. Chem. Phys.* **2005**, *7*, 3297-3305.

[8] F. Weigend, F. Accurate Coulomb-Fitting Basis Sets for H to Rn. *Phys. Chem. Chem. Phys.* **2006**, *8*, 1057-1065.

[9] Gaussian 09, Revision D.01, M. J. Frisch, G. W. Trucks, H. B. Schlegel, G. E. Scuseria, M. A. Robb, J. R. Cheeseman, G. Scalmani, V. Barone, B. Mennucci, G. A. Petersson, H. Nakatsuji, M. Caricato, X. Li, H. P. Hratchian, A. F. Izmaylov, J. Bloino, G. Zheng, J. L. Sonnenberg, M. Hada, M. Ehara, K. Toyota, R. Fukuda, J. Hasegawa, M. Ishida, T. Nakajima, Y. Honda, O. Kitao, H. Nakai, T. Vreven, J. A. Montgomery, Jr., J. E. Peralta, F. Ogliaro, M. Bearpark, J. J. Heyd, E. Brothers, K. N. Kudin, V. N. Staroverov, T. Keith, R. Kobayashi, J. Normand, K. Raghavachari, A. Rendell, J. C. Burant, S. S. Iyengar, J. Tomasi, M. Cossi, N. Rega, J. M. Millam, M. Klene, J. E. Knox, J. B. Cross, V. Bakken, C. Adamo, J. Jaramillo, R. Gomperts, R. E. Stratmann, O. Yazyev, A. J. Austin, R. Cammi, C. Pomelli, J. W. Ochterski, R. L. Martin, K. Morokuma, V. G. Zakrzewski, G. A. Voth, P. Salvador, J. J. Dannenberg, S. Dapprich, A. D. Daniels, O. Farkas, J. B. Foresman, J. V. Ortiz, J. Cioslowski, and D. J. Fox, Gaussian, Inc., Wallingford CT, 2013.

[10] Staroverov, V. N.; Scuseria, G. E.; Tao, J.; Perdew, J. P. Comparative Assessment of a New Nonempirical Density Functional: Molecules and Hydrogen-Bonded Complexes. *J. Chem. Phys.* **2003**, *119*, 12129.

[11] Dunning, Jr., T. H. Gaussian Basis Sets for Use in Correlated Molecular Calculations. I. The Atoms Boron Through Neon and Hydrogen. *J. Chem. Phys.* **1989**, *90*, 1007-1023.

[12] Davidson, E. R. Comment on "Comment on Dunning's Correlation-Consistent Basis Sets" *Chem. Phys. Lett.* **1996**, *260*, 514-518.

[13] Momma, K.; Izumi, F. VESTA 3 for Three-Dimensional Visualization of Crystal, Volumetric and Morphology Data. *J. Appl. Crystallogr.* **2011**, *44*, 1272-1276.

[14] Phillips, J. C.; Braun, R.; Wang, W.; Gumbart, J.; Tajkhorshid, E.; Villa, E.; Schulten; K. Scalable Molecular Dynamics with NAMD. *J. Comp. Chem.* **2005**, *26*, 1781-1802.

[15] Darden, T.; York, D.; Pedersen, L. Particle Mesh Ewald: An N·log(N) Method for Ewald Sums in Large Systems. *J. Chem. Phys.* **1993**, *98*, 10089-10092.

[16] Vanommeslaeghe, K.; Raman, E. P.; MacKerell, Jr., A. D. Automation of the CHARMM General Force Field (CGenFF) II: Assignment of Bonded Parameters and Partial Atomic Charges. *J. Chem. Inform. Modeling* **2012**, *52*, 3155-3168.

[17] Vanommeslaeghe, K.; MacKerell Jr. A. D. Automation of the CHARMM General Force Field (CGenFF) I: Bond Perception and Atom Typing. *J. Chem. Inform. Modeling* **2012**, *52*, 3144-3154.

[18] *PetaChem*. 2011: p. http://www.petachem.com

[19] Humphrey, W.; Dalke, A.; Schulten, K. VMD: Visual Molecular Dynamics. *J. Molec. Graphics* **1996**, *14*, 33-38.

[20] Gray, H. B.; Maverick, A. W. Solar Chemistry of Metal Complexes. *Science* **1981**, *214*, 1201-1205.

[21] Connelly, N. G.; Geiger, W. E. Chemical Redox Agents for Organometallic Chemistry. *Chem. Rev.* **1996**, *96*, 877-910.